**Title**

CHARGED E-HYPERON PRODUCTION AND DECAY: ENERGETICS, LIFETIMES, AND BRANCHING RATIOS



**Author**

Dyer, John.

**Publication Date**

1960-11-01

Thesis/dissertation

UCRL9450

# UNIVERSITY OF CALIFORNIA

# Ernest O. Lawrence Radiation Laboratory

## CHARGED Σ-HYPERON PRODUCTION AND DECAY: ENERGETICS, LIFETIMES, AND BRANCHING RATIOS

## DISCLAIMER

UCRL-9450
UC-34 Physics and Mathematics
TID-4500 (15th Ed.)

UNIVERSITY OF CALIFORNIA

Lawrence Radiation Laboratory
Berkeley, California

Contract No. W-7405-eng-48

# CHARGED Σ- HYPERON PRODUCTION AND DECAY: ENERGETICS, LIFETIMES, AND BRANCHING RATIOS

John N. Dyer

(Ph. D. Thesis)

November 1, 1960

Printed in USA. Price $2.00. Available from the
Office of Technical Services
U. S. Department of Commerce
Washington 25, D.C.

# CHARGED Σ-HYPERON PRODUCTION AND DECAY: ENERGETICS, LIFETIMES, AND BRANCHING RATIOS

Contents

# CHARGED Σ- HYPERON PRODUCTION AND DECAY: ENERGETICS, LIFETIMES, AND BRANCHING RATIOS

John N. Dyer

Lawrence Radiation Laboratory
University of California
Berkeley, California

November 1, 1960

ABSTRACT

Charged Σ hyperons produced by negative K-meson interactions at rest with emulsion nuclei have been studied. New estimates of the masses and lifetimes are presented, based upon range measurements of the pions involved in Σ production and decay. Such data have not previously been available. Statistical improvements were obtained in the $\Sigma^+$ mass and lifetime determined by the proton decay mode, and the $\Sigma^- - \Sigma^+$ mass difference determined by $K^-$ absorptions on free protons. With the one exception noted below, the new data are compatible with previous results.

The mass of the $\Sigma^+$ hyperon, determined by its decay at rest, is

$M_{\Sigma^+}$ = 1189.33 ± 0.22 Mev (using 80 protons from $\Sigma^+ \rightarrow p + \pi^0$), and

$M_{\Sigma^+}$ = 1188.75 ± 0.54 Mev (using 26 pions from $\Sigma^+ \rightarrow n + \pi^+$).

These data were combined to yield $M_{\pi^0}$ = 134.0 ± 1.0 Mev, the first direct estimate of the mass of the neutral particle involved in the proton decay mode.

From 56 $K^- + p \rightarrow \Sigma^\pm + \pi^\mp$ interactions with free protons, the following data were obtained from the hyperon ranges:

$\Sigma^- - \Sigma^+$ range difference = 106.9 ± 4.3 μ (32 $\Sigma^-$, 16 $\Sigma^+$),

$\Sigma^- - \Sigma^+$ mass difference = 6.32 ± 0.25 Mev,

$M_{\Sigma^-} = (M_{\Sigma^+} + \Delta M)$ = 1195.65 ± 0.33 Mev,

$M_{K^-}$ = 493.61 ± 0.33 Mev.

In addition, 3 $\pi^-$ mesons and 13 $\pi^+$ mesons were followed to rest in emulsion. The average momentum of the $\pi^+$ is found to be 2.76 ±0.64 Mev/c less than that of the $\Sigma^-$; the anomaly has not been explained. The average momentum of the $\pi^-$ is compatible with that of the $\Sigma^+$.

The mass of the $\Sigma^-$ hyperon has been measured by using 11 decays in flight, and is 1196.0 ± 1.1 Mev. This is compatible with the value obtained from the mass-difference method.

Energy spectra of the $\Sigma^+$ and $\Sigma^-$ hyperons emitted from complex nuclei indicate that approx 18% of the $\Sigma^-$ and approx 9% of the $\Sigma^+$ are produced by multinucleon $K^-$-capture processes. The lifetime of the $\Sigma^+$ hyperon, as determined from its proton decay mode, is

$\tau^+ = 0.85^{+0.15}_{-0.11} \times 10^{-10}$ sec using 107 decays at rest and in flight, and

$\tau^+ = 0.86^{+0.75}_{-0.27} \times 10^{-10}$ sec using 43 decays in flight only.

Lifetimes determined from the pion decay modes, using events at rest and in flight, are

$$\tau^+ = 0.80^{+0.14}_{-0.11} \times 10^{-10} \text{ sec, and}$$

$$\tau^- = 1.75^{+0.39}_{-0.30} \times 10^{-10} \text{ sec.}$$

The best value for the $\Sigma^+$ lifetime calculated from both decay modes is

$$\tau^+ = 0.82^{+0.10}_{-0.08} \times 10^{-10} \text{ sec.}$$

When only decays in flight via the pion modes are considered, the lifetimes are depressed, but experimental biases are detected and discussed.

The following branching ratios have been found:

$$\frac{\Sigma^+ \rightarrow p + \pi^0}{\text{all } \Sigma^+} = 0.50 \pm 0.03 \text{ ,}$$

$$\frac{\Sigma^+ \rightarrow p + \gamma}{\Sigma^+ \rightarrow p + \pi^o} = \frac{0}{95} ,$$

$$\frac{\Sigma^\pm \rightarrow \text{leptons}}{\Sigma^\pm \rightarrow \pi^+} = \frac{0}{129} ,$$

$$\frac{\Sigma^- \rightarrow \text{leptons}}{\Sigma^- \rightarrow \pi^-} = \frac{0}{67} .$$

# I. INTRODUCTION

Charged $\Sigma$ hyperons produced by $K^-$ - meson interactions were first observed in 1955 by Hornbostel and Salant.[1] Following their observations, techniques for producing particle beams containing $K^-$ mesons advanced rapidly, and by the end of the year several experiments had been performed which revealed some of the properties of the new particles.[2,3] In 1956, $K^-$ interactions at rest with free protons were observed both in emulsions and in bubble chambers, and it was realized that a $\Sigma^- - \Sigma^+$ mass difference exists.[4,5] Data accumulated rapidly as "enriched" $K^-$ - meson beams were developed.[6] Bubble chamber and emulsion groups both began intensive studies of the $K^-$ interactions and of the hyperons which they produce. The masses, lifetimes, and principal decay modes of the hyperons were soon well established. The values of these, as of November 1957, have been summarized by Barkas and Rosenfeld[7] and have not changed significantly since, except for a slight decrease in the $\Sigma^-$ mass resulting from improved measurements of the $\Sigma^- - \Sigma^+$ mass difference.[8]

In several respects, however, the existing data are unsatisfactory or incomplete: (a) An apparent discrepancy has persisted between the lifetime calculated from $\Sigma$ decays in flight into charged pions in emulsion and the lifetime of the $\Sigma^+$ as calculated in bubble chambers or from the proton decay mode in emulsion. In particular, emulsion studies have consistently indicated a lower lifetime.[9-19] The existence of an unknown particle of short lifetime has been suspected. (b) The leptonic decay modes of $\Sigma$ hyperons, predicted by a generalized universal Fermi interaction, are so far undetected.[20-22] (c) The energies of the pions involved in $\Sigma$ decay and production processes have not been accurately measured.

In Part I of this paper a series of measurements is presented which overdetermine the hyperon masses. The $\Sigma^+$ mass is measured by both the $\Sigma^+ \rightarrow p + \pi^0$ and $\Sigma^+ \rightarrow n + \pi^+$ decay modes, and the data combined to yield a direct estimate of the mass of the neutral particle involved in the proton decay mode. The $\Sigma^-$ mass is determined by analysis of its decay in flight via $\Sigma^- \rightarrow n + \pi^-$ as well as by the $\Sigma^- - \Sigma^+$ mass difference. The reaction $K^- + p \rightarrow \Sigma^{\pm} + \pi^{\mp}$ is studied in detail, and an anomaly is found concerning the momentum of the $\pi^+$ meson. From this reaction the mass of the $K^-$ meson is determined in terms of the other masses and the hyperon momentum. With the exception noted, all these measurements give consistent results. Finally, the energy spectra of $\Sigma^-$ and $\Sigma^+$ hyperons emitted from complex nuclei are presented and an estimate of the frequency of multinucleon $K^-$ capture is deduced.

Part II is concerned with hyperon lifetimes. Consistent values for the $\Sigma^+$ lifetime have been obtained by using both the proton and pion decay modes, and the $\Sigma^-$ lifetime is measured with much greater accuracy than previously possible with emulsion techniques. It is found, however, that decays in flight into charged pions yield a low value for both the $\Sigma^+$ and $\Sigma^-$ lifetimes. Biases which cause this are detected and discussed.

Several branching ratios are determined in Part III. The decays $\Sigma^+ \rightarrow p + \gamma$ and $\Sigma \rightarrow$ leptons are found to be absent in the sample of hyperons observed. Decays of the $\Sigma^+$ into charged and neutral pions are found to occur with equal frequency.

A discussion of particle velocity measurements by means of track ionization is appended.

## II. OUTLINE OF EXPERIMENTAL PROCEDURES

### A. The Emulsion Stacks

All the $\Sigma$ hyperons used in this work were created by the interactions at rest of $K^-$ mesons with emulsion nuclei. Five emulsion stacks were utilized in order to obtain sufficient data for the analyses that follow. All of these were exposed to $K^-$-meson beams from the Bevatron, but at different times and with different techniques. The stacks are briefly described in the following table; more information can be found in the references listed.

| Stack | Pellicle dimensions (inches) | Number of Pellicles | Emulsion type | References |
|---|---|---|---|---|
| 1U | 3 X 6 | 120 | G-5, 600μ | 23, 24 |
| 2D | 3 X 6 | 108 | K-5, 600μ | 25, 26 |
| M | 6 X 9 | 246 | G-5, 600μ | — |
| 2B | 9 X 12 | 240 | G-5, 600μ | 23-25 |
| A | 6 X 9 | 216 | K-5, 600μ | 27 |

The 1U, 2B, and M stacks were exposed to similar beams. Selection of $K^-$ mesons was accomplished by degrading and then magnetically analyzing a portion of the negative particle flux from the Bevatron target. In the 1U and 2B stacks, the mesons penetrate approx 3 cm into the emulsion before coming to rest, while in the M stack additional degrading before the stack reduced the penetration to less than 1 cm.

The Murray coaxial velocity spectrometer[28] was utilized for the exposures of the 2D and A stacks. The mesons penetrate approximately to the center of each stack before coming to rest. The emulsions in both of these are unusually free of random background grains and spurious tracks.

### B. Scanning Techniques

The $K^-$ stars were located either by following tracks into the emulsion from their entrance points at the edge of the stack (1U, 2B, and M stack) or by searching a prescribed region in each pellicle where the $K^-$ mesons were known to come to rest (2D and A stacks). The tracks followed into the edge-scanned stacks were selected by establishing appropriate criteria regarding their ionization and direction as they entered the emulsion. High efficiencies for rejecting unwanted background particles were obtained; in the 2B stack, for example, 90% of the tracks followed were caused by $K^-$ mesons. This method of scanning selects $K^-$ stars without bias regarding their terminal behavior. The samples of stars collected from the A and 2D stacks, however, suffered from just such a bias — namely, an observational loss of interactions that did not produce dark prongs.

Regardless of how they are found, $K^-$ interactions can be utilized as a source of charged $\Sigma$ hyperons. These appear as proton-like tracks originating at the $K^-$ star. The initial velocity of a hyperon produced by a $K^-$ interaction at rest is limited by conservation of energy to a maximum value corresponding to about 2.5 times the minimum of ionization, or a range of about 8 cm. If a pion is also produced by the interaction, a more stringent limit is imposed and the maximum $\Sigma$ range is reduced to about 1 cm. These figures allow for the motion of nucleons within a complex nucleus and represent the limiting values to be expected from $K^-$ captures on two nucleons and a single nucleon, respectively. Even at these limits, $\Sigma$ hyperons always appear as dark tracks.

The procedures followed to locate the $\Sigma$ hyperons in the various stacks are listed below.

1U and 2B Stacks: All dark prongs from 1- and 2-pronged stars were followed to their terminations. Dark tracks from larger stars were not followed beyond the surface of the pellicle in which they originated, and their terminations were noted only if they occurred in that pellicle. The hyperons found are therefore biased toward those that terminate for some reason near the parent star; data from these stacks are not used in the lifetime calculations.

A Stack: The bias mentioned above was removed by following all dark prongs to their terminations regardless of the size of the parent star. The results of this effort are shown in Table I. Because this was an area-scanned stack, zero-pronged stars are not included in the table, nor has any correction been made for an observational loss of fast pions that would tend to alter the classifications shown in the table. This correction is discussed in Part II of this paper, and it is shown there that less than 8% of near-minimum tracks were missed.

2D and M Stacks: These were used only for the data they furnished concerning the reactions $K^- + p \rightarrow \Sigma^\pm + \pi^\mp$.

Detailed discussions of the criteria established for recognizing $\Sigma$ - hyperon events among the dark prongs followed will be found in appropriate sections of Parts III, IV, and V.

## C. Data Recording

All data are recorded on 8-1/2 X 11-inch McBee Keysort cards of the sort shown in Fig. 1. The holes across the top of the card are used to describe the $K^-$ interaction, and the holes along the sides to describe any star prongs that are of interest. When an event is found, a card is started; the observer sketches the event and notes its location in the emulsion, punches the appropriate holes to describe the star, and has a physicist or experienced scanner verify his conclusions and initial the card. Each $K^-$ interaction is listed on a separate card, which then forms a permanent record of the event. Additional data on the same event are verified and entered on the card as they become available. Results of measurements can be written on either face of the card, along with explanatory comments.

This system has been in use now for more than two years and has proved workable.

Table I

Identification of dark prongs from stars in the A stack

| Type of K- Star[a] | Identification of Dark Prongs $\Sigma^+$ | $\Sigma^-$ | $\Sigma^\pm$ | HF | Stable Prong | Number of Stars | Number of $\Sigma$'s |
|---|---|---|---|---|---|---|---|
| $1\pi$ | - | - | - | - | - | 106 | 0 |
| 1 | 14 | 8 | 5 | 0 | 208 | 235 | 27 |
| 2 | 19 | 5 | 7 | 9 | 567 | 304 | 31 |
| $2\pi$ | 84 | 21 | 0 | 3 | 235 | 343 | 105 |
| 3 | 22 | 10 | 13 | 21 | 930 | 332 | 45 |
| $3\pi$ | 25 | 4 | 1 | 8 | 344 | 191 | 30 |
| 4 | 12 | 6 | 2 | 13 | 1025 | 248 | 20 |
| $4\pi$ | 7 | 3 | 0 | 8 | 420 | 146 | 10 |
| 5 | 4 | 2 | 4 | 16 | 774 | 160 | 10 |
| $5\pi$ | 4 | 3 | 0 | 11 | 294 | 78 | 7 |
| 6 | 0 | 3 | 1 | 9 | 305 | 53 | 4 |
| $6\pi$ | 0 | 0 | 0 | 2 | 183 | 37 | 0 |
| $> 6$ | 0 | 1 | 2 | 8 | 227 | 34 | 3 |
| $> 6\pi$ | 0 | 0 | 0 | 10 | 86 | 16 | 0 |
| Total | 191 | 66 | 35 | 118 | 5598 | 2284 | 292 |

[a]The number indicates the number of star prongs. Pi ($\pi$) indicates that one of the prongs is a $\pi$ meson.

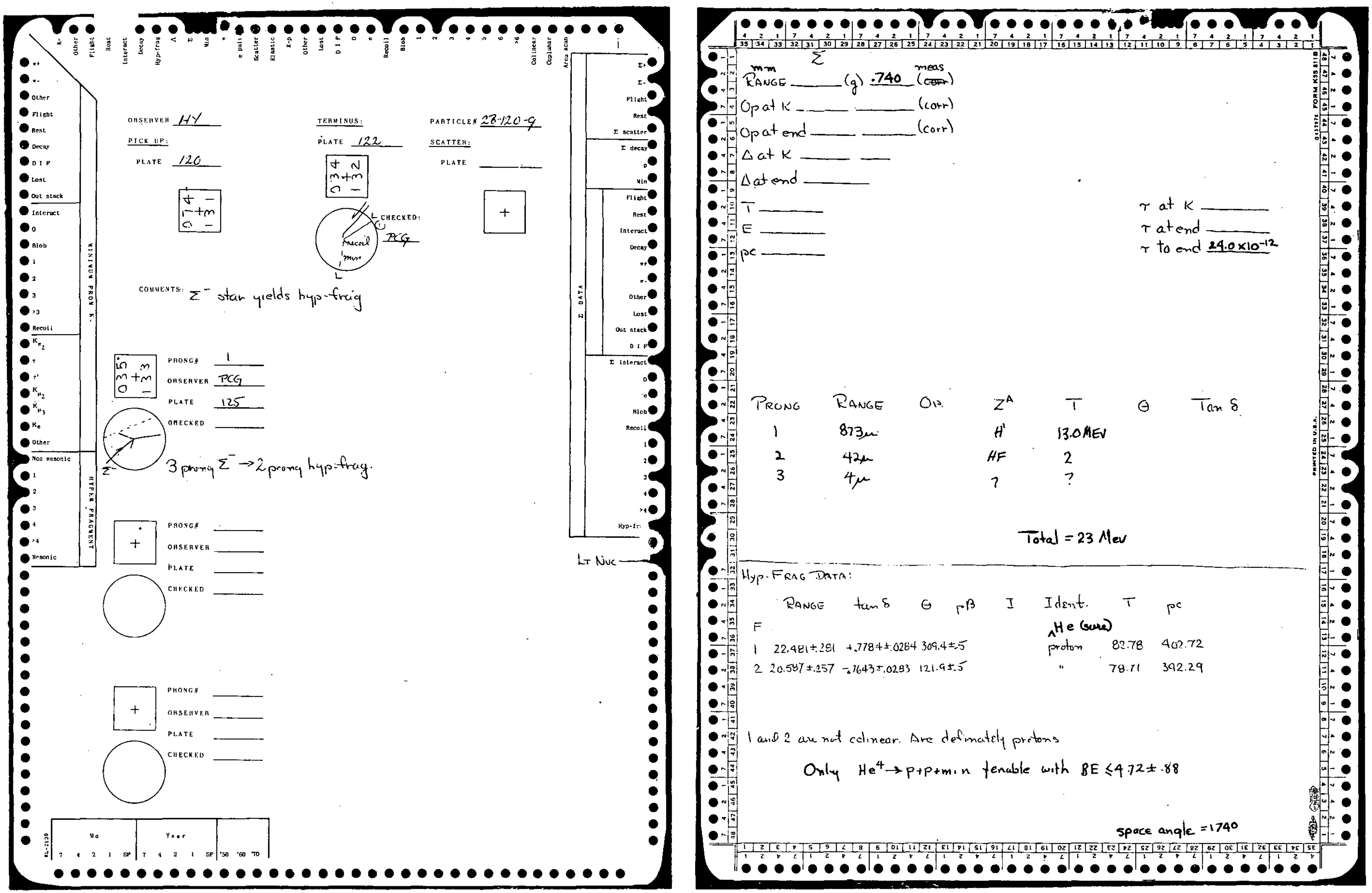


MUB-218

Fig. 1. Example of Keysort card used for recording data.

## III. ENERGETICS AND MASS VALUES

The energy of a charged particle in nuclear emulsion is determined most accurately by measuring its range and comparing this range with a standard range-energy relation.[29] The measured ranges must be adjusted by corrections which allow for the shrinkage of emulsion after processing and for variations of density found between different manufacturer's batches. The techniques employed are discussed below.

### A. Range Measurement

To measure the length of a track in emulsion, one may use a microscope equipped to measure translations along three mutually perpendicular axes. Ordinarily, the microscope stage is defined as the x-y plane and movement along the x and y axes is effected by means of carefully machined lead screws. A pellicle placed on the stage lies in the x-y plane. Lengths in the z direction, defined as the optic axis of the microscope, are measured by displacements of the microscope objective. The distance between two points in an emulsion pellicle is determined by their coordinates in the orthogonal frame thus established. Alternately, one may measure distances in the x-y plane with a calibrated reticle placed in an eyepiece so as to be superimposed upon the field of view.

An automated microscope,[30] equipped to punch coordinate data on cards suitable for the IBM 650, was used to measure most tracks whose length was $> 1$ mm. Inaccuracies in the lead screws of this device did not permit its use for shorter tracks. Tracks less than 1 mm long (and all hyperon tracks) were measured by the "reticle method." The reticles used spanned about 130 $\mu$ in the field of view (with $10\times$ oculars and $100\times$ objective) and were calibrated to better than 1 part in 1500.

Because of multiple scattering, the "true" range of a particle cannot be measured; it is, rather, approximated by a series of straight-line segments whose end points are chosen according to some convention. The convention used here was the same as that used in establishing the range-energy relation; that is, a new segment was started whenever the track had changed direction by an amount $\geq 5$ deg. Ranges measured in this way are less than 0.1% short of the true ranges, and no error is introduced in determining the energy from the range-energy relation.

## B. Shrinkage Factor

To obtain the range of a particle in unprocessed emulsion, a correction must be introduced which multiplies all vertical dimensions by a factor equal to the ratio of the unprocessed pellicle thickness to the thickness at the time measurements are made. Pellicles when scanned are about half as thick as when exposed, a collapse in the vertical dimension having taken place because of the removal of part of the constituents of the emulsion during processing.

The following procedure for determining the shrinkage factor was used for all the stacks except the M stack. Before processing, a sample of pellicles was taken and the density of each measured. After processing, the area of each was measured and the unprocessed mean thickness calculated. The mean processed thickness was then measured and the shrinkage factor determined for each pellicle of the sample selected. Finally, one or more standard reference points were selected and thickness measurements made on each processed pellicle at these points. It is assumed that pellicles processed together have the same shrinkage factor. Therefore, the original pellicle thickness at the reference points can be calculated from the shrinkage factors measured in the sample. It is important that all the thickness measurements above be performed under the same conditions of humidity so that they do not change during the course of the measurements.

The unprocessed thickness of each pellicle at the reference points having been determined, the shrinkage factor at any future time can be determined by measuring the pellicle thickness at these points and finding the ratio with the original thickness. Fluctuations in thickness, which occur because of the absorption and evaporation of water by the pellicle as ambient humidity changes, do not introduce errors into the shrinkage factors so determined.

The procedure followed for the M stack was similar, but the density of each pellicle was measured and the unprocessed thickness determined with a micrometer, the measured points serving as reference points for thickness measurements.

## C. Emulsion Density

The stopping power of emulsion is a function of its density. The range-energy relation, then, is valid only for emulsion of standard density, which is defined to be 3.815 g/cc. Ranges measured in emulsions of different density must be adjusted to the value they would have had in standard emulsion before reference can be made to a range-energy relation.

Variations of emulsion density occur primarily because of the absorption of water vapor, since the stopping power of water is much less than that of emulsion. The variation of proton range with emulsion density is shown in Fig. 2.

Precise determinations of emulsion densities were made by weighing the pellicles in air and in carbon tetrachloride. The error was estimated to be 0.1%. All but the two smallest stacks contained pellicles from more than one manufacturer's batch. An average density for each batch was calculated from the samples measured in that batch. These results are presented in Table II.

## D. Corrections to the Measured Ranges

The measured range of a particle in a single pellicle is calculated from the formula

$$R = \sum_i \left\{ (x_{i+1} - x_i)^2 + (y_{i+1} - y_i)^2 + \left[ S(z_{i+1} - z_i) \right]^2 \right\}^{1/2} ,$$

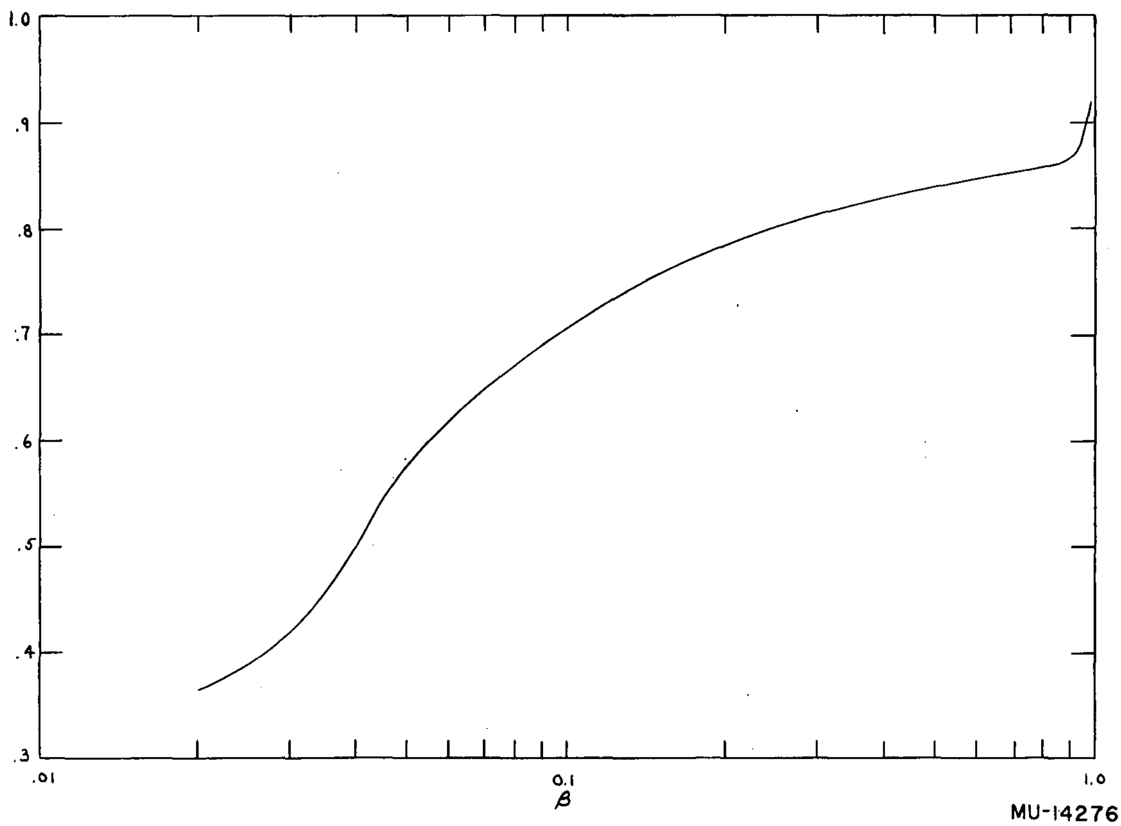


Fig. 2. Variation of proton range with emulsion density. The percent range decrease per percent density increase above the standard density of 3.815 g/cc is plotted against the velocity (β) of the particle.

Table II

Emulsion densities

| Stack | Batch densities (g/cc) |
|---|---|
| 1U | 3.810 ± 0.003 |
| 2D | 3.839 ± 0.003 |
| 2B | 3.821 ± 0.003 |
| | 3.814 |
| | 3.816 |
| | 3.830 |
| | 3.803 |
| | 3.807 ± 0.003 |
| A | 3.837 ± 0.003 |
| | 3.822 ± 0.003 |
| M | 3.845 ± 0.003 |
| | 3.820 |
| | 3.823 |
| | 3.835 ± 0.003 |

where $x_i$, $y_i$, and $z_i$ are the coordinates of the ith point recorded along the track. Because S, the shrinkage factor, changes from day to day according to variations in relative humidity, its value must be determined at the time the range is measured. Our procedure is to include thickness measurements of the pellicle at the reference points as part of any measurement into which the shrinkage factor enters. The correct value of S is then calculated as described previously. If the reticle method is used, the x and y terms are replaced by $L_i^2$, where $L_i$ is the distance in the x-y plane between the ith and (i+1) th z measurements. The total range of a particle is the sum of the ranges in each pellicle.

The corrections made for emulsion-density variations are based upon Fig. 2 and the data of Table II. These typically amount to a few tenths of a percent of the measured ranges. Each track must be considered separately because the correction used depends upon those particular pellicles through which the particle passes as well as upon the initial velocity of the particle. The ranges corrected in this way are said to be normalized to the conditions for which the range-energy relation is valid.

Statistical errors in the range measurements arise from range straggling and from measurement error. The latter is estimated to be 1/2% in the case of pions of about 8 cm range and 1% for protons and $\Sigma$ hyperons measured by the reticle method. These figures are the result of repeated measurements by different observers. The magnitude of range straggle in emulsion has been tabulated by Barkas et al.[31] It ranges from 2.6% for pions of 9 cm range to 1.4% for $\Sigma$ hyperon of 700 $\mu$ range.

Systematic errors can be introduced by the shrinkage factor and density measurements. The latter introduces a fractional range error of the same order of magnitude as the fractional error in density; about 1 part in 1000. The effect of a shrinkage-factor error depends upon the dip angle of the track. The error in S is reflected into the range according to the formula $\Delta R/R = (\Delta S/S) \sin^2\delta$, where $\delta$ is the angle of inclination in unprocessed emulsion measured with respect to the emulsion surface. The shrinkage-factor uncertainty is estimated to be 2% in the A stack and 1% in the other stacks.

## E. Mass of the $\Sigma^+$ Hyperon

The decay at rest of the $\Sigma^+$ hyperon by either of the processes $\Sigma^+ \rightarrow p + \pi^0$ or $\Sigma^+ \rightarrow n + \pi^+$ furnishes sufficient information for calculation of the $\Sigma^+$ mass. Both these decay modes produce pictures in emulsions characterized by a secondary track originating at the terminus of a proton-like prong from a $K^-$ star. A secondary proton of range about 1680 $\mu$ indicates the proton decay mode. The efficiency for detecting such events is taken to be 100% throughout this paper.

The neutron decay mode presents more problems to the observer. The emitted pion is near the minimum of ionization and may escape detection. In addition, the decay $\Sigma^- \rightarrow n + \pi^-$ may occur when the $\Sigma^-$ is near the end of its range and can be confused with $\Sigma^+ \rightarrow n + \pi^+$ at rest. Typically, a decay in flight can be distinguished from a decay at rest by the appearance of the hyperon track only if the residual range at the decay point is $> 200\ \mu$. The charge of the hyperon may be established in two ways. If the pion track can be followed, and the pion identified by its terminal behavior, then the hyperon is assigned the same charge as the pion. In addition, if the $K^-$ interaction also produces a charged pion (a "$\pi$ partner") and the charge of this pion can be determined, the hyperon is assigned the opposite charge. The latter rests upon the assumption that production is via $K^- + p \rightarrow \Sigma^{\pm} + \pi^{\mp}$ and that charge-exchange interactions do not confuse the identification. No case was found in which the hyperon and the pion had the same charge.

In principle, it is necessary only (a) to determine the momentum of the charged decay product by measuring its range, (b) to assign the same momentum to the neutral product, and (c) to calculate the mass from the equation

$$M_{\Sigma^+} = (M_0^2 + P^2)^{1/2} + (M^2 + P^2)^{1/2} , \qquad (1)$$

where $M_0$ is the mass of the neutral product and $M$ is the mass of the charged product. In practice, however, the decay $\Sigma^+ \rightarrow n + \pi^+$ supplies inferior data because the greater range straggle of the pion increases the number of events needed to obtain a given accuracy. Also, the pion range is long enough (about 9 cm) to cause a considerable fraction of these to leave the emulsion stacks or suffer a catastrophe before coming to rest.

## 1. The Decay $\Sigma^+ \rightarrow p + \pi^0$ at Rest

Fifty events in the A stack, 14 in the 1U stack, and 16 in the 2B stack have been used to calculate a mean proton range according to the formula

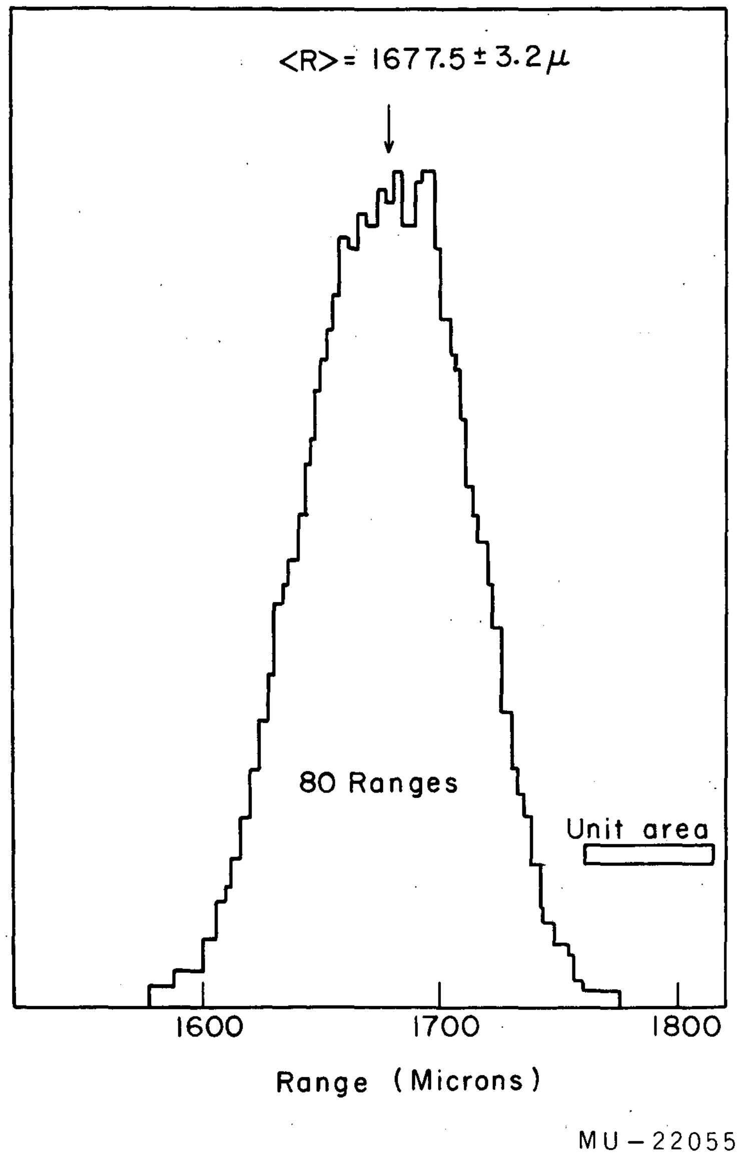


Fig. 3. Proton range ideogram for 80 protons from $\Sigma^+ \to p + \pi^0$ decays at rest in the A, 2B, and 1U stacks.

$$\langle R \rangle = \left( \sum_i \frac{R_i}{(\Delta R_i)^2} \right) \Bigg/ \left( \sum_i \frac{1}{(\Delta R_i)^2} \right). \qquad (2)$$

The weighting factors, $\Delta R_i$, are the uncertainties in the ranges and are compounded from the following independent errors:

(a) 1.4% Bohr range straggle;
(b) 1.0% measurement error; and
(c) shrinkage factor uncertainty.

The mean ranges and their external errors calculated from Eq. (2) are

| | |
|---|---|
| 1678.5 ± 4.4 μ | (A stack), |
| 1671.2 ± 8.0 μ | (2B stack), |
| 1680.5 ± 9.0 μ | (1U stack), |
| 1677.5 ± 3.2 μ | (combined). |

Figure 3 shows the normalized range distribution for all 80 protons. The spread of the distribution is 1.43% or 28 μ ; straggle alone predicts a spread of 24 μ. The internal and external estimates of the error are both ± 3.2 μ.

Using now the Barkas 1957 range-energy relation, one finds that the mean range corresponds to a proton of energy 18.85 Mev. The uncertainty in energy may be obtained from the uncertainty in range by noting that the energy varies with the range according to a power law, $T \propto R^{\eta}$, where $\eta$ is about one-half.[29] The uncertainty in range is obtained by compounding the statistical uncertainty and the systematic uncertainty in the range-energy relation. The latter is estimated to be 0.3% in this region. The relation

$$\left(\frac{\Delta T}{T}\right) = \eta \left[ \left(\frac{\Delta R}{R}\right)_S^2 + \left(\frac{\Delta R}{R}\right)_{RE}^2 \right]^{1/2} \qquad (3)$$

gives $\Delta T/T = 0.2\%$, where $\eta = 0.573$ and the subscripts S and RE indicate statistical and range-energy, respectively.

The $\Sigma^+$ mass may now be calculated from Eq. (1), using the following input data:

| | | |
|---|---|---|
| Proton range | = | $1677.5 \pm 3.2\ \mu$, |
| Proton energy | = | $18.85 \pm 0.04$ Mev, |
| Proton momentum | = | $189.01 \pm 0.20$ Mev/c, |
| Proton mass | = | $938.213 \pm 0.01$ Mev, |
| $\pi^0$ meson mass | = | $135.00 \pm 0.05$ Mev. |

The result of this calculation is

$$M_{\Sigma^+} = 1189.33 \pm 0.22 \text{ Mev.}$$

It is adopted as the best estimate of the $\Sigma^+$ mass for this paper.*

2. <u>The Decay $\Sigma^+ \to n + \pi^+$ at Rest</u>

Twenty-one pions from these decays were followed to rest and their ranges measured. Two of these were in the 2B stack and 19 in the A stack. Another five pions left the A stack with residual ranges less than 5 mm, as determined by ionization measurements. These 26 ranges were used to make another estimate of the $\Sigma^+$ mass.

The mean range was calculated from Eq. (2) with uncertainties compounded from

(a) 2.6% Bohr range-straggle;
(b) 0.5% measurement error;
(c) shrinkage factor uncertainties; and
(d) uncertainty in residual range for 5 events.

---

*The value, $M_{\Sigma^+} = 1189.40 \pm 0.20$ Mev, given by Barkas and Rosenfeld[8] includes the data of this thesis. The average value for the other references in their paper is $M_{\Sigma^+} = 1189.48 \pm 0.24$ Mev, and is based on a total of 68 events.

The mean range and its external error is 92.484 ± 0.490 mm. Figure 4 shows the normalized range distribution. The spread of the distribution is 2.5%, or 2.31 mm — slightly less than expected from straggle alone. The internal estimate of the error is ± 0.44 mm.

The energy corresponding to the mean range is 91.72 ± 0.44 Mev, the error being calculated as before, but with the systematic uncertainty in the pion range-energy relation set at 0.5%. The quantities pertinent to the mass calculation are

| | | |
|---|---|---|
| Pion range | = | 92.484 ± 0.490 mm, |
| Pion energy | = | 91.72 ± 0.44 Mev, |
| Pion momentum | = | 184.44 ± 0.55 Mev/c, |
| Neutron mass | = | 939.506 ± 0.01 Mev. |

These data yield

$$M_{\Sigma^+} = 1188.75 \pm 0.54 \text{ Mev.}$$

This mass value is less than that obtained from the proton decay mode by an amount 0.58 ± 0.63 Mev. Although the results are consistent, a small error in the range-energy relation for pions of range approx 9 cm may contribute to the difference. If the pion energy were 92.19 Mev — a value 0.5% greater than that obtained from the range-energy relation — the calculated $\Sigma^+$ mass would become 1189.33 Mev.

## F. The Mass of the Neutral Particle in the Proton Decay Mode

Although the assumption that a $\pi^0$ meson is emitted in the proton decay mode of the $\Sigma^+$ hyperon is supported by indirect evidence (e.g., by the presence of Dalitz pairs at the $\Sigma^+$ decay vertex),[32] no direct measurement of the mass of the neutral particle has been reported.

Such a measurement can be made by combining the $\Sigma^+$ mass determined from $\Sigma^+ \rightarrow n + \pi^+$ decays with the proton energy from the proton decay mode. The mass of the neutral particle is then given by the equation

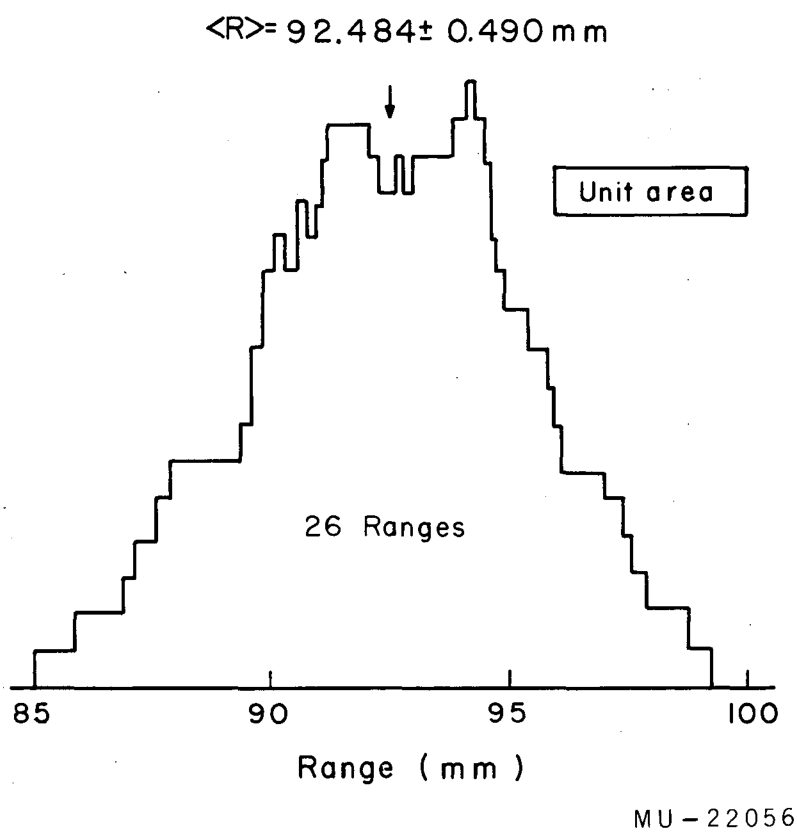


Fig. 4. Pion range ideogram for 26 pions from $\Sigma^+ \rightarrow n + \pi^+$ decays at rest. All but two of the events are in the A stack.

$$M^{o} = \left[(M_{\Sigma} - M_{p})^{2} - 2M_{\Sigma}T_{p}\right]^{1/2} = 134.0 \pm 1.0 \text{ Mev.}$$

This value is compatible with the $\pi^{o}$ meson mass.[8] It is assumed throughout this paper that the decay mode $\Sigma^{+} \rightarrow p + \pi^{o}$ is correct.

### G. The Reaction $K^{-} + p \rightarrow \Sigma^{\pm} + \pi^{\mp}$

The captures of $K^{-}$ mesons at rest by hydrogen atoms in emulsion provide valuable data for mass determinations. Since the reaction takes place with a free (not bound) nucleon, the energies of the products can be simply related to the masses involved. The mass difference between the $\Sigma^{+}$ and $\Sigma^{-}$ hyperons can be calculated from the resulting difference in their ranges. The mass of any one of the products can be determined from its range and the range-energy relation if the momentum of its partner is known. Finally, the reaction Q value and the $K^{-}$-meson mass are fixed if the momentum of either product can be measured and the mass of the partner is known.

#### 1. Identification of Events

The presence of one of these reactions is signaled by a star from which two prongs emerge in exactly opposite directions. The prongs are strikingly different in appearance. The track of the hyperon is heavily ionized, while that of the pion is near the minimum of ionization. Such stars are commonly known as collinear events. Before being accepted as an instance of a $K^{-}$ absorption by hydrogen, an event must satisfy all three of the following criteria: (a) the tracks of the hyperon and pion must be collinear, (b) the hyperon range must be compatible with one of the reactions, and (c) the star must not show evidence of a recoil, a "blob," or Auger electrons. Failure to satisfy any of these requirements indicates that the reaction did not take place with a free nucleon. It is conceivable, however, that a reaction with a complex nucleus could satisfy these criteria, particularly if the $K^{-}$ meson is captured by a peripheral nucleon. To investigate this

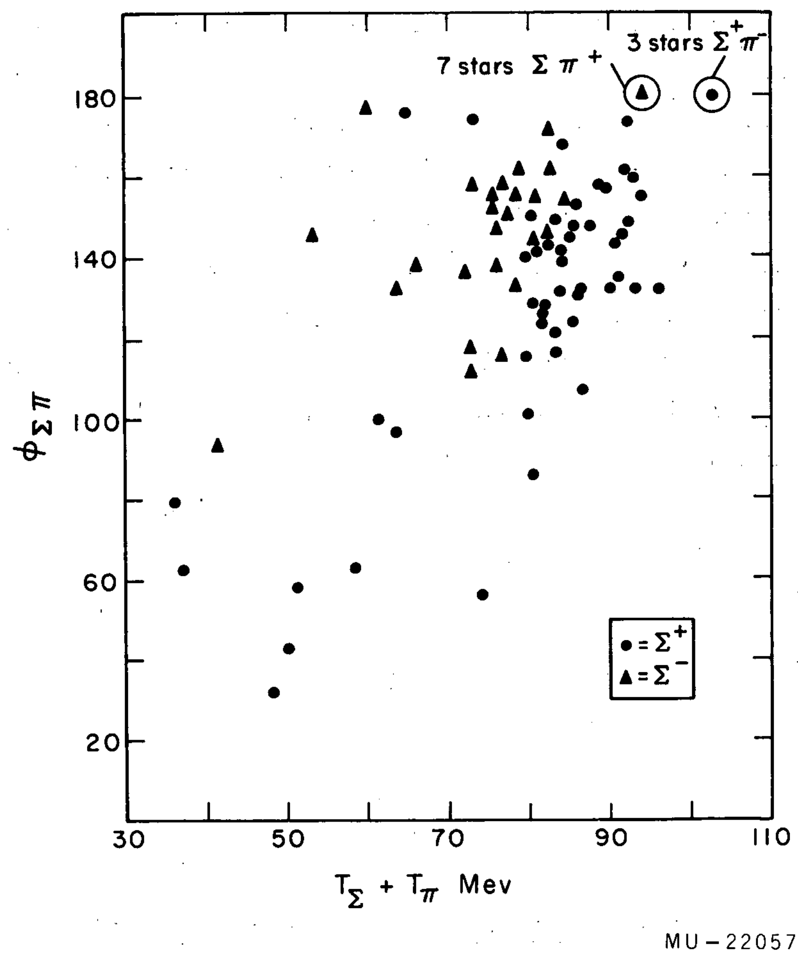


Fig. 5. Plot of the space angle between the Σ hyperon and its π partner versus the sum of their kinetic energies. Ten collinear events are confined to the regions shown.

possibility, a study was made in the A stack of all two-pronged stars that emitted a hyperon and a pion. In Fig. 5, the sum of the kinetic energies of the products is plotted against the angle formed by their tracks at the $K^-$ star. It is clear from this plot that the collinear events form well-defined groups clearly separated from other two-pronged stars. Figure 6 is a similar plot with only the hyperon energy considered. The collinear events again form distinct groups. It is apparent from these data that the selection criteria do define a unique class of events. The probability of forming a pseudo-collinear star by interaction with a complex nucleus is negligible.

Unfortunately, the collinear events are rare, only one occurring for about every two hundred interactions with complex nuclei. The sample gathered for this study includes events in all five stacks, distributed among them as follows:

| Stack | $\Sigma^+\pi^-$ | $\Sigma^-\pi^+$ |
|---|---|---|
| 1U | 0 | 1 |
| 2D | 6 | 5 |
| 2B | 2 | 5 |
| M | 5 | 19 |
| A | 3 | 10 |
| | 16 | 40 |

## 2. The Hyperon Ranges: $\Sigma^+ - \Sigma^-$ Mass Difference

The $\Sigma^+$ and $\Sigma^-$ hyperons from collinear events do not have the same mean range, a fact which may be attributed to the $\Sigma^+ - \Sigma^-$ mass difference and used to calculate it. The range-difference is insensitive to the $K^-$ mass and to errors in the range-energy relation, although not completely independent of either. An exact relation connecting the mass difference and the range difference can be written in terms of the range-energy index and the known masses.

To avoid systematic range errors introduced by faulty reticle calibrations or the peculiarities of an individual microscope, the range

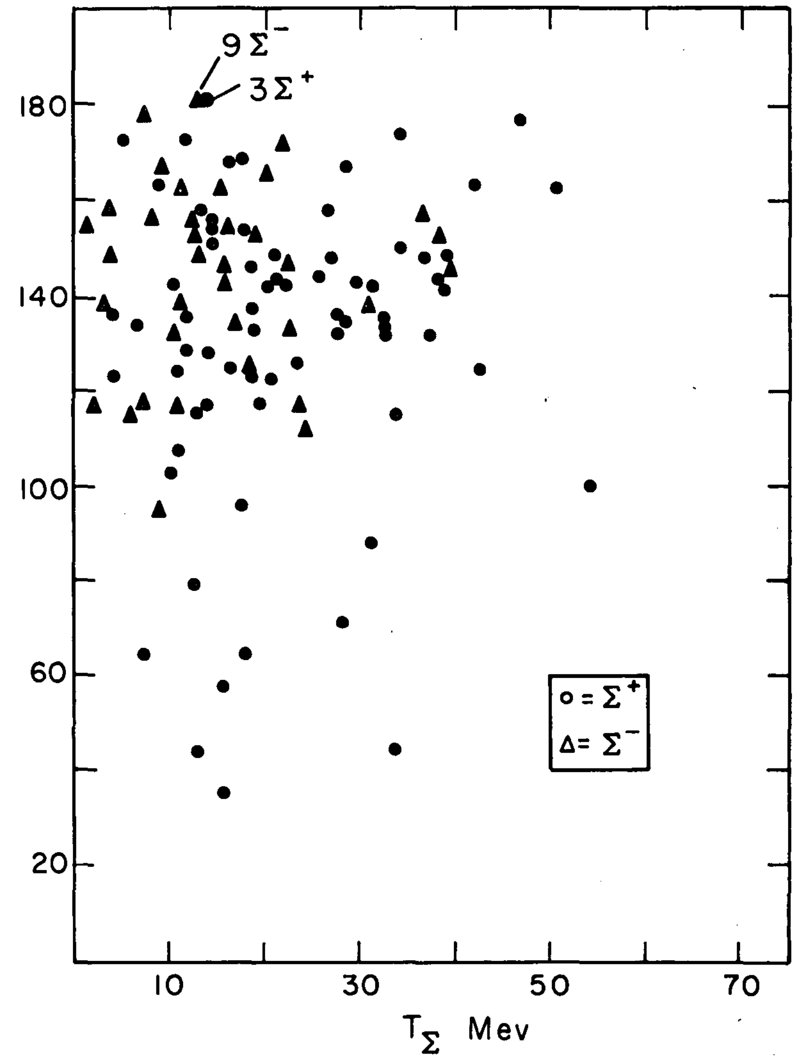


MU-22058

Fig. 6. Plot of the space angle between the Σ hyperon and its π partner versus the Σ kinetic energy. Nine $\Sigma^-$ and three $\Sigma^+$ from the collinear events are confined to the regions shown.

of each hyperon was measured by at least three different observers, each of whom used his "own" microscope and reticle. If the three measurements differed by more than 1% , additional measurements were made. The termination of the track of a $\Sigma^+$ hyperon is accurately defined by the origin of its decay product. Negative hyperons, however, interact when they come to rest. A considerable fraction of these interactions produce either a small one-prong star or produce no star at all. Therefore, it is sometimes impossible to tell whether a deflection near the end of a track represents (a) a small star with one prong, or (b) a scattering followed by an interaction which produces no star. To avoid errors, only those $\Sigma^-$ tracks that had unambiguous terminations were included in the calculation of the mean $\Sigma^-$ range.

Mean ranges were calculated according to Eq. (2) with weighting factors compounded from

(a) 1.2% Bohr range-straggle;
(b) 1.0% measurement error; and
(c) shrinkage factor uncertainties.

The normalized mean ranges are

$\Sigma^+$ : $817.7 \pm 3.7\ \mu$ (16 ranges);
$\Sigma^-$ : $710.8 \pm 2.2\ \mu$ (32 ranges).

Figure 7 shows the normalized range distribution. For the $\Sigma^-$ ranges the internal estimate of the error is $\pm 2.2\ \mu$; for the $\Sigma^+$ ranges it is $\pm 3.4\ \mu$. Range straggle in both cases is about $10\ \mu$, while the distribution width in both is about $13\ \mu$, the additional spread arising from measurement and shrinkage-factor errors.

The range and mass differences are

$$\Delta R = 106.9 \pm 4.3\ \mu,$$
$$\Delta M = 6.32 \pm 0.25 \text{ Mev}.$$

The $\Sigma^-$-hyperon mass is now determined by the equation

$$M_{\Sigma^-} = (M_{\Sigma^+} + \Delta M) = 1195.65 \pm 0.33 \text{ Mev}.$$

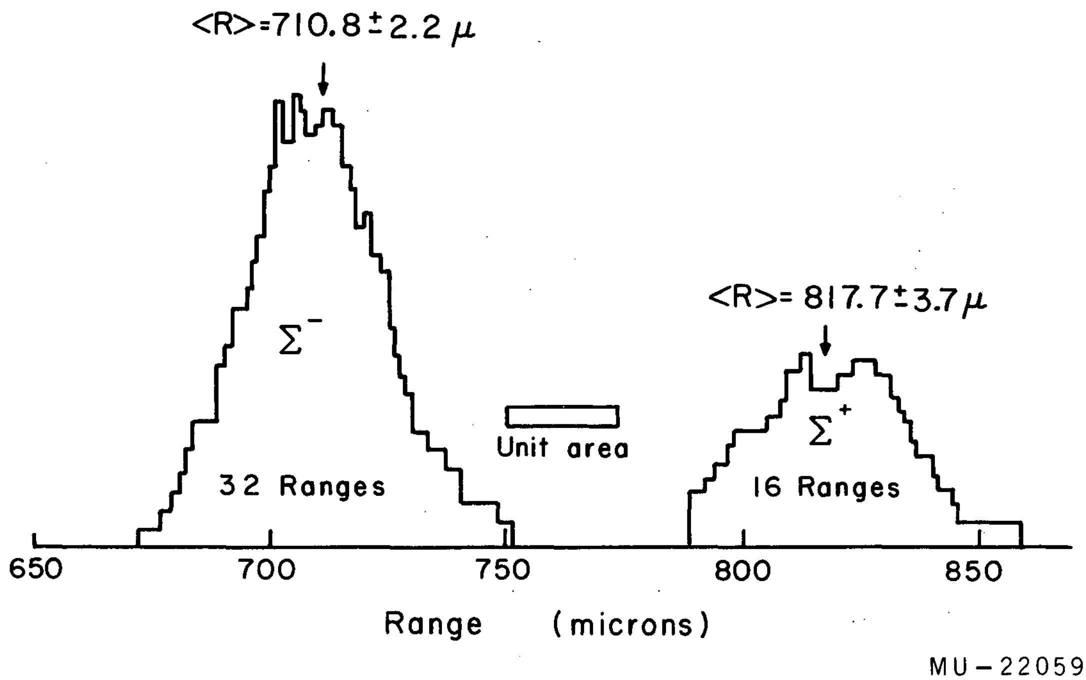


Fig. 7. The $\Sigma^+$ and $\Sigma^-$ ranges from the collinear events. Only $\Sigma^-$ tracks with unambiguous endings are included. The range difference is $106.9 \pm 4.3\ \mu$.

The quantities determined for the hyperons were as follows:

| | $\Sigma^+$ | $\Sigma^-$ |
|---|---|---|
| Mass | 1189.33 ± 0.22 Mev | 1195.65 ± 0.33 Mev |
| Range | 817.7 ± 3.7 μ | 710.8 ± 2.2 μ |
| Energy | 13.73 ± 0.04 Mev | 12.67 ± 0.03 Mev |
| Momentum | 181.24 ± 0.27 Mev/c | 174.52 ± 0.21 Mev/c |

Energies were calculated by using the recent corrections to the range-energy relation published by Heckman et al.[33] Equation (3) was used to calculate the errors in energy, the systematic range uncertainty being taken as 0.25%.

3. Mass of the $K^-$ Meson

The $K^-$ mass can be calculated from the expression

$$M_K = \left[M_\Sigma^2 + P_\Sigma^2\right]^{1/2} + \left[M_\pi^2 + P_\Sigma^2\right]^{1/2} - M_p , \quad (4)$$

where $P_\Sigma$ is the measured value of the $\Sigma^+$ momentum and $M_\Sigma$ is the $\Sigma^+$ mass. The result of the calculation is

$$M_K = 493.61 \pm 0.33,$$

which is compatible with the latest published value, 493.9 ± 0.2 Mev, given by Barkas and Rosenfeld.[8]

4. The Pion Ranges: An Anomaly

Measurement of the pion ranges was undertaken for the sake of completeness, even though the above data already showed satisfactory consistency. Relatively few pions can be used for range determination; many suffer inelastic collisions in flight or fail to come to rest in the emulsion. From 56 collinear events, only 3 $\pi^-$ and 13 $\pi^+$ ranges could be measured. These ranges were measured on the automated microscope in exactly the manner described for the pions from

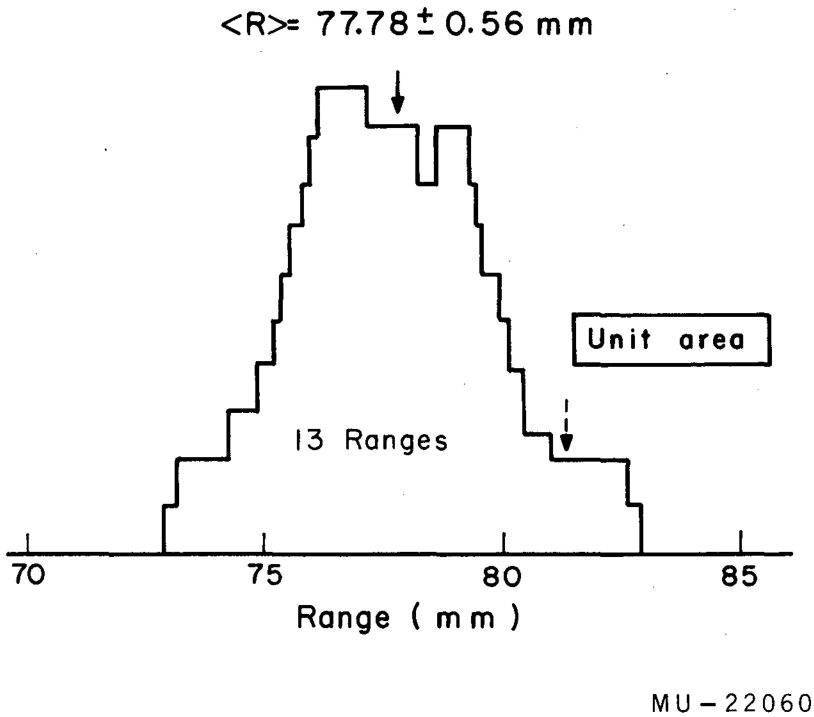


Fig. 8: $\pi^+$ range ideogram for 13 $\pi^+$ mesons from $K^- + p \rightarrow \Sigma^- + \pi^+$ at rest. The arrow at 81.3 mm indicates the range expected for the energy calculated from the reaction.

$\Sigma^+$ decays. Equation (2) was used to calculate the weighted mean ranges, with the $\Delta R_i$ compounded from the errors as before but with 2.6% Bohr range straggle. The range-energy relation and Eq. (3) again furnished the corresponding energies and energy errors. The systematic error in the range-energy relation was taken to be 0.5%.

The quantities thus obtained are:

| | $\pi^+$ | $\pi^-$ |
|---|---|---|
| Range | 77.78 ± 0.56 mm | 88.87 ± 1.44 mm |
| Energy | 81.74 ± 0.44 Mev | 89.32 ± 0.94 Mev |
| Momentum | 171.76 ± 0.60 Mev/c | 181.45 ± 1.18 Mev/c |

Comparing these values with those obtained for the hyperons, one sees that in the reaction $K^- + p \rightarrow \Sigma^+ + \pi^-$ the measured momenta of the products are in accord. On the other hand, the $\Sigma^-$ and $\pi^+$ momenta differ by 2.76 ± 0.64 Mev/c. This discrepancy may indicate an error in one or more of the following: the range measurements, the $\Sigma^-$ mass, or the range-energy relation. These are discussed below, and it is shown that reasonable errors in these quantities do not remove the discrepancy.

a. The $\pi^+$ Ranges

The normalized range distribution of the 13 $\pi^+$ mesons is shown in Fig. 8. The distribution width is ± 1.8 mm or ± 2.3% , a value somewhat less than the expected 2.6% Bohr range straggle. The internal estimate of the error of the mean is consequently less than the external, the values being 0.50 mm and 0.56 mm, respectively. This tightness of distribution indicates that the statistical range errors are not larger than expected. The mean value, however, is 3.52 mm short of the expected value of 81.30 mm predicted by the range-energy relation for a pion of momentum 174.52 Mev/c.

As a first step in checking for systematic errors, the ranges were calculated separately for each of the three stacks involved:

| | | |
|---|---|---|
| A stack | (7 ranges) | 77.43 ± 0.77 mm, |
| M stack | (5 ranges) | 78.20 ± 0.90 mm, |
| B stack | (1 range ) | 77.94 ± 2.00 mm. |

There is no significant difference among these. In the A stack, it was possible to check for shrinkage-factor errors by plotting the ranges of protons from $\Sigma^+ \rightarrow \pi^o + p$ decays at rest against their dip angles. Such a plot indicates that the shrinkage factors are not in error by more than ± 1.0%. Moreover, the pion ranges are not sensitive to small errors in the shrinkage factors; a systematic increase of 1% in all of the shrinkage factors increases the mean range by only 0.2% or 0.17 mm.

The second step was to compare the measured ranges with estimates of ranges made by reference to the grid system printed on each pellicle. A schematic representation of a track can be constructed by plotting the points at which a particle passes from one pellicle to another as it proceeds through the emulsion stack, and assigning to each pellicle its original thickness. The mean range obtained in this way is 78.35 mm, a value which must be compared to the unweighted mean of the measured ranges, 77.78 mm. The difference is 0.7%, and can be accounted for by the small air gap that existed between the pellicles when they were exposed. The same procedure, applied to the pions from $\Sigma^+ \rightarrow \pi^+ + n$ decays, gave similar results.

Finally, the automated microscope itself was checked by remeasuring on it the pion tracks used to establish the range-energy relation at pion ranges of approx 3.7 cm and approx 7.6 cm. The results were in complete agreement with the original (1957) measurements.[34]

b. <u>The $\Sigma^-$ Mass</u>

It is interesting to consider the effect of changing the $\Sigma^-$ mass. Figure 9 is a schematic representation of the situation. The band marked "$\Sigma^-$ momentum" shows the measured value and its uncertainty (± 1 standard deviation) as derived from the range-energy relation with the $\Sigma^-$ range fixed at 710.8 ± 2.2 μ. This is, of course, a function of the $\Sigma^-$ mass, plotted along the horizontal axis. The band "pion momentum" has similar meaning. The two dashed lines represent the expected value of the momentum as a function of the $\Sigma^-$ mass, calculated for two values of the $K^-$ mass. Finally, the horizontal bars represent the values of the $\Sigma^-$ mass reported in this paper. Note that the $\Sigma^-$ momentum at $M_\Sigma$ = 1195.65 Mev corresponds to a $K^-$ mass of approx 493.6 Mev, in agreement with the previous calculation. Two different values of the $\Sigma^-$ mass will be considered.

<u>$M_\Sigma$ = 1198.2 Mev.</u>: At this value the expected momentum agrees with the measured pion momentum if the $K^-$ mass is 493.6 Mev. The measured $\Sigma^-$ momentum has risen to almost 175 Mev/c, however, making the discrepancy greater than before. At the expected value of momentum, the $\Sigma^-$ would have a range of about 668 μ, a value far short of the observed range.

If this mass value represented an excited state of the hyperon which would decay isotropically somewhere in the first few microns of its range according to $\Sigma^* \rightarrow \Sigma^- + \gamma + 2.5$ Mev, the mean range of the $\Sigma^-$ would remain near 668 μ. Moremore, the decay would result in a spread in ranges extending from approx 640 μ to approx 710 μ for γ emission parallel and antiparallel to the $\Sigma^*$ momentum. Only if the γ were constrained in some way to emission in the backward direction would the experimental range distribution for the $\Sigma^-$ be obtained. I cannot see any reason why this should be so.

<u>$M_\Sigma$ = 1168.0 Mev.</u>: At this value the measured hyperon and pion momentum agree. This mass, however, is not consistent with

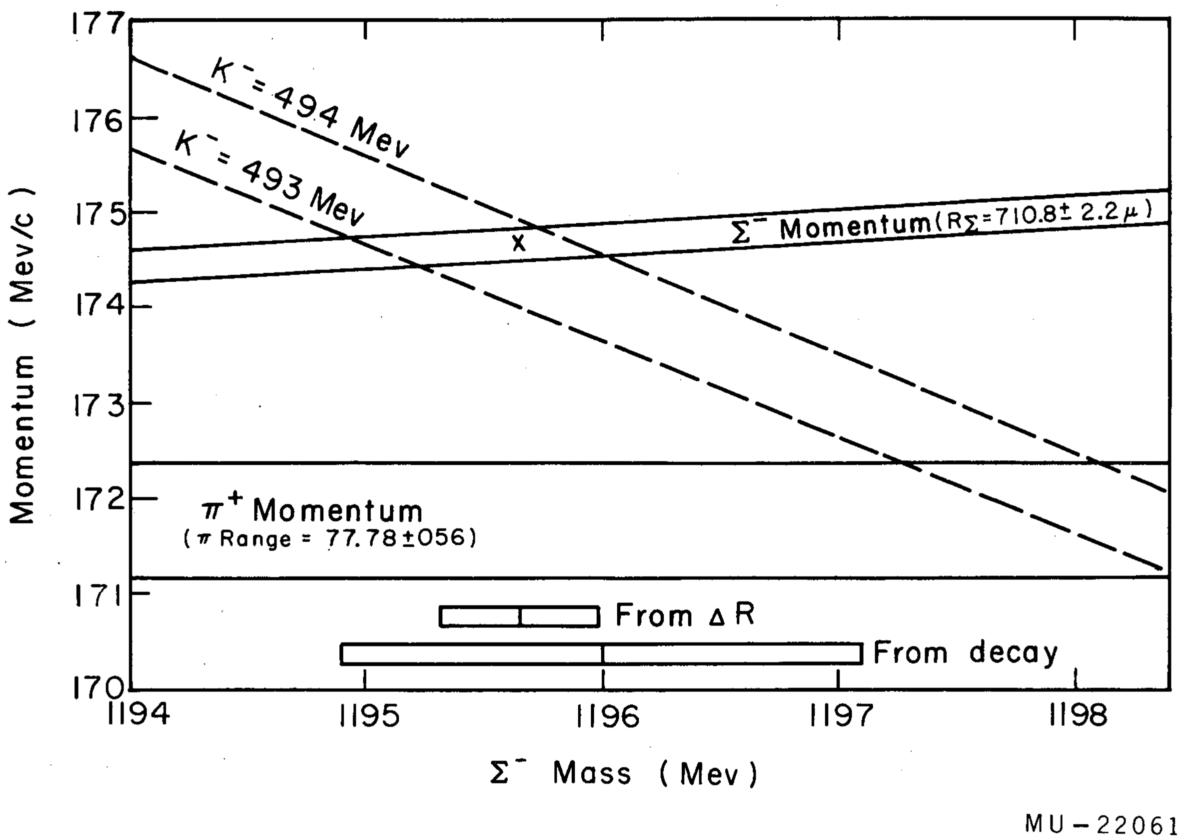


Fig. 9. Relationships between calculated and measured quantities in the reaction $K^- + p \rightarrow \Sigma^- + \pi^+$ plotted as a function of the $\Sigma^-$ mass. The two momentum bands are the measured values. The dashed lines are the calculated values for two choices of the $K^-$ mass.

any previous measurements, nor are the momenta in agreement with the value expected if the $K^-$ mass is near 494 Mev.

c. The $\Sigma^-$ Range

The effect of changing the $\Sigma^-$ range can be visualized by displacing the band "$\Sigma^-$ momentum" in Fig. 9. As the range decreases, the point at which the observed and expected momenta agree moves toward higher values of the $\Sigma^-$ mass. The mass needed is just that which would be calculated from the altered value of the range difference, keeping the $\Sigma^+$ range fixed. Thus, if the range were reduced from $711 \pm 2\ \mu$ to approx $668\ \mu$, the mass calculation would lead to $M = 1198.2$ Mev.

Evans et al.[17] have reported a mean $\Sigma^-$ range of $696 \pm 6\ \mu$, a $\Sigma^+ - \Sigma^-$ range difference of $128 \pm 9\ \mu$, and a mass difference of $7.46 \pm 0.56$ Mev. The $\Sigma^-$ mass is therefore $1196.8 \pm 0.7$ Mev, and its momentum from the range-energy relation is $173.6 \pm 0.4$ Mev/c. This agrees with the expected value for $M_K$ approx 493.7.

Decreasing the $\Sigma^-$ range decreases the discrepancy in the pion and hyperon momenta, but to get complete agreement in this way requires that the range be reduced to approx $668\ \mu$.

d. The Range-Energy Relation

It was noted in the discussion of $\Sigma^+ \rightarrow \pi^+ + n$ decays that the energy given by the range-energy relation could be in error by about 0.5% for pions of approx 9 cm range. The pions from $K^- + p \rightarrow \Sigma^- + \pi^+$ are expected to have energy equal to 83.84 Mev if the $K^-$ mass is 493.6 Mev and the $\Sigma^-$ mass is 1195.65 Mev. The energy corresponding to their range, however, is $81.74 \pm 0.44$ Mev, which differs from the expected value by 2.5%. A systematic error of this magnitude for pions of range approx 8 cm is not reasonable.

Unfortunately, because of the long range of the pions and the scarcity of sufficiently large emulsion stacks, there are no

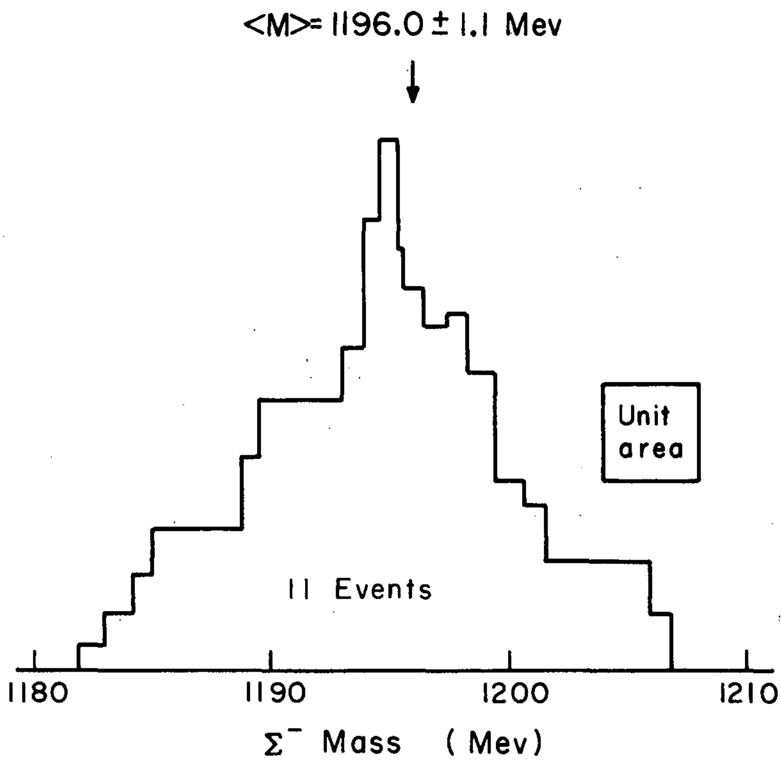


MU-22062

Fig. 10. $\Sigma^-$ mass value ideogram for the 11 masses determined by analysis of the $\Sigma^-$ decay in flight.

published data to confirm or deny these measurements. The least radical assumption is that the pion ranges are in error, but the difference between measured and expected values is greater than can be accounted for by corrections which we consider reasonable. An additional indication that the pion ranges are at fault may be had by calculating the $K^-$ mass with the pion momentum substituted into Eq. (4). The result of the calculation is $M_K = 490.1 \pm 0.6$. This value is not compatible with the accepted $K^-$ mass.

### H. The $\Sigma^-$ Mass by the Decay $\Sigma^- \rightarrow \pi^- + n$

Because of the anomaly in the reaction $K^- + p \rightarrow \Sigma^- + \pi^+$, it is desirable to measure the $\Sigma^-$ mass in a way independent of this reaction. In emulsion, the only alternative method is the decay in flight of the $\Sigma^-$ hyperon via $\Sigma^- \rightarrow \pi^- + n$.

The pion ranges, the laboratory angle between the $\Sigma$ and the $\pi$, and the $\Sigma$ velocity are the quantities needed to determine the $\Sigma$ mass. Eleven decays were selected for analysis. Most of these were very near the ends of their ranges when they decayed and were selected because the pion was emitted in a direction such that its energy was not sensitive to the $\Sigma^-$ velocity. Ionization measurements were used to estimate the hyperon velocities.

Figure 10 shows the distribution of calculated mass values. The error on each value was obtained by combining the uncertainties in velocity, angle, and pion energy. The weighted mean value is

$$M_{\Sigma^-} = 1196.0 \pm 1.1 \text{ Mev.}$$

This value is in good agreement with the mass obtained from the collinear events.

### J. The Hyperon Energy Spectra

The kinetic energies of the hyperons observed in the A stack are shown in Figs. 11 and 12. The energies of those particles which

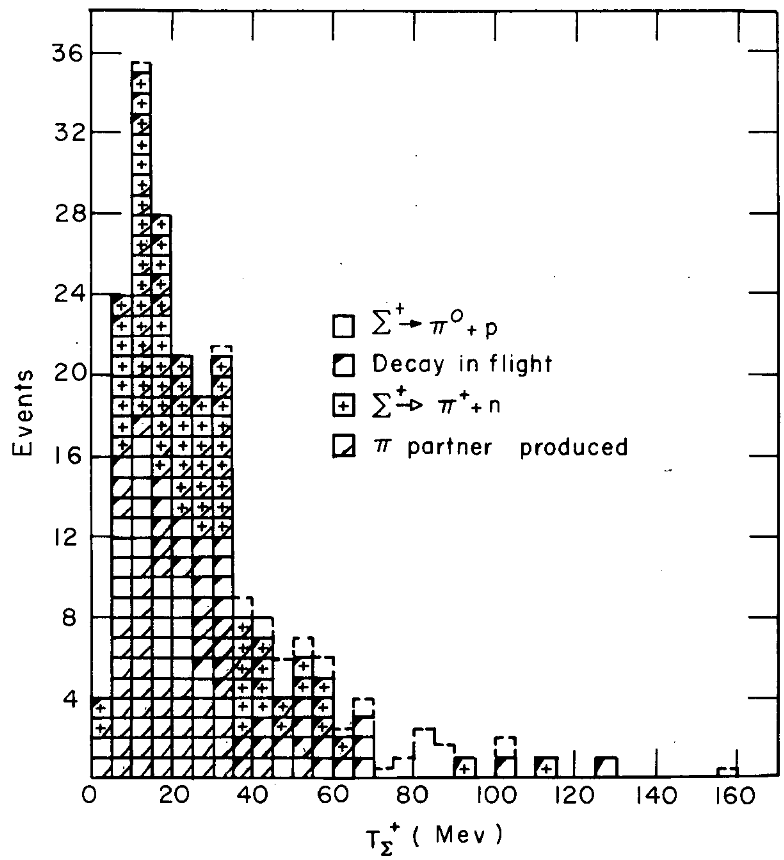


MU-22063

Fig. 11. $\Sigma^+$ kinetic energy distribution in the A stack. The dashed outline indicates the probable assignment of 35 $\Sigma \rightarrow \pi + n$ decays in flight of unknown charge.

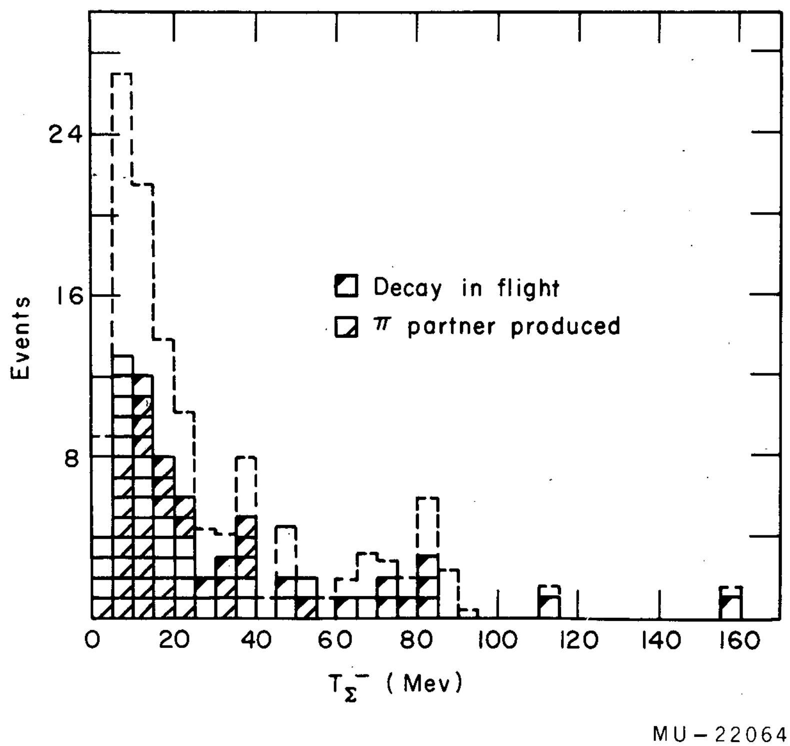


Fig. 12. $\Sigma^-$ kinetic energy distribution in the A stack. The dashed outline represents the correction for unseen $\Sigma^-$ interactions at rest and the probable assignment of 35 $\Sigma \rightarrow \pi + n$ decays of unknown charge.

decayed in flight were determined either by kinematic analysis — the range and angle of emission of the decay product — or by ionization measurements on the hyperon tracks. Some features of the distributions are:

(a) No hyperon of kinetic energy > 60 Mev is produced with a $\pi$ partner. Since approx 60 Mev represents the upper limit of energy for production by $K^-$ absorption on a single nucleon, the more energetic particles are produced by multinucleon $K^-$ captures.

(b) The average energies for the observed particles are 25.6 Mev for $\Sigma^+$ that decay by the proton mode, 26.2 Mev for $\Sigma^+$ that decay by the pion mode, and 28.9 Mev for the $\Sigma^-$. For the $\Sigma^-$, the true value of average energy will be somewhat lower than the figure given, because of the severe observational loss of $\Sigma^-$ stars at rest.

1. Multinucleon $K^-$ Captures

The fraction of $K^-$ captures proceeding through multinucleon channels can be estimated from the number of hyperons produced with energy >60 Mev. Two corrections must be made to the observed distributions before an estimate is made:

(a) The number of $\Sigma^-$ interactions at rest in each energy interval is multiplied by 3.17 to correct for the number of $\Sigma^-$ stars that were not observed. This factor is derived on page 62.

(b) Thirty-five decays in flight by the pion modes with undetermined charge must be added. This has been done by giving each decay a weight in each spectrum defined by the probabilities that they be $\Sigma^+$ or $\Sigma^-$ hyperons. These probabilities are derived on page 61. The energy distributions after these adjustments are shown by the dashed lines in Figs. 11 and 12.

Evans et al.[35] have calculated that for two-nucleon $K^-$ captures, approx 87% of the $\Sigma^+$ and approx 74% of the $\Sigma^-$ hyperons should be produced with energies greater than 60 Mev. Therefore, for the corrected energy distributions, we have approx 18 % of the $\Sigma^-$ produced by two-nucleon interactions, and approx 9% of the $\Sigma^+$ hyperons produced similarly. It is assumed here that reactions on more than two nucleons are rare compared to the number on two. These are, of course, rough estimates. Interactions of the hyperons inside the nucleus could severely distort the observed energy distributions if the interaction cross sections were strongly energy-dependent. Further, no correction has been made for the number of hyperons that interact in flight, because it is not possible to determine the number accurately. Approximately 6.5 meters of heavy-particle track was scanned in the A stack, and 33 interactions in flight were noted. This is not incompatible with the number of proton interactions expected. Five of these, however, appeared to be exothermic reactions, indicating hyperons. A reasonable limit of the order of 10 hyperon interactions in flight can be assumed, and this number does not affect the conclusions drawn above.

## K. Summary and Discussion of Data

The mass of the $\Sigma^+$ hyperon as determined by the decay mode $\Sigma^+ \rightarrow p + \pi^0$ has now been measured with accuracy approaching the limit imposed by the uncertainties in the range-energy relation and in the $\pi^0$ meson mass. If the statistical uncertainty in the mean proton range were reduced to zero, the error quoted in the $\Sigma^+$ mass would be reduced by only 0.02 Mev, from 0.22 Mev to 0.20 Mev.

Other values reported for the $\Sigma^+$ mass are summarized in the table below. All were determined with essentially the same techniques as described in this paper.

| Mass (Mev) | Number of decays | Reference |
|---|---|---|
| 1189.0 ± 0.5 | 6 | 17 |
| 1189.4 ± 0.4 | 29 | 36 |
| 1190.1 ± 0.5 | 7 | 37 |
| 1189.1 ± 0.5 | 10 | 38 |
| 1189.28 ± 0.32 | 31* | 23 |
| 1189.33 ± 0.22 | 80 | This paper |

*These events are included in the 80 events reported in this paper.

The measurement of the $\Sigma^+$ mass by the decay mode $\Sigma^+ \rightarrow n + \pi^+$ has not previously been attempted. The value of the $\pi^o$ meson mass obtained by combining the data from the two decay modes therefore represents the first direct measurement of the mass of the neutral particle involved in the $\Sigma^+ \rightarrow p + \pi^o$ decay.

The reactions $K^- + p \rightarrow \Sigma^{\pm} + \pi^{\mp}$ have been studied by several groups to obtain values for the $\Sigma^- - \Sigma^+$ mass difference. The most important results are as follows.

| Mass difference (Mev) | Data | Reference |
|---|---|---|
| 7.46 ± 0.56 | 14 events; $4\Sigma^+$, $10\Sigma^-$ | 17 |
| 8.12 ± 1.48 | 2 events; $1\Sigma^+$, $1\Sigma^-$ | 39 |
| 6.90 ± 1.00 | 3 events; $1\Sigma^+$, $2\Sigma^-$ | 36 |
| 6.56 ± 0.66 | 7 events; $3\Sigma^+$, $4\Sigma^-$* | 23 |
| 6.32 ± 0.25 | 48 events; $16\Sigma^+$, $32\Sigma^-$ | This paper |

The present data represent a significant statistical improvement over the measurements previously available.

The pion ranges from these reactions have not previously been measured, therefore there are no published data to substantiate or deny the pion range anomaly found.

The $\Sigma^-$ mass measurement from the analysis of decays in flight reported here represents the first emulsion determination of this mass not dependent upon the mass difference method.

---

*These events are included in the 48 events reported in this paper.

## IV. HYPERON LIFETIME MEASUREMENTS

It is now well established that the $\Sigma^+$ and $\Sigma^-$ hyperons do not decay at the same rate, and that the $\Sigma^+$ rate is approximately twice that of the $\Sigma^-$.[7,8] But for several years, some difficulties have persisted concerning the decay rates when measured in emulsion, and the possibility existed that an unknown body of short life was present.[15] In particular, efforts to measure an average decay rate by using samples containing both $\Sigma^+$ and $\Sigma^-$ decays in flight via the pion modes consistently indicated a "mixed" rate greater than that of the $\Sigma^+$, as determined by its proton-decay mode. Moreover, emulsion and bubble-chamber estimates of the $\Sigma^+$ lifetime have not been in very impressive agreement, although not inconsistent. For these reasons, new measurements of these quantities were undertaken.

### A. The Maximum-Likelihood Method

The method used to estimate the lifetimes is that of Maximum Likelihood, first presented by Bartlett and applied to cloud-chamber events, and later extended by others to emulsions.[16,40-42] Two different likelihood functions can be written, one considering only those particles which decay in flight, and the other considering in addition those that come to rest. Hyperons produced by $K^-$ interactions at rest in emulsion typically have moderation times of the same order as their lifetimes; somewhat less than half of them are observed to decay in flight. Therefore, either likelihood expression can be used to estimate the lifetimes.

If both decays in flight and hyperons that come to rest before decaying are considered, the most likely decay rate is defined as that value which makes the expression

$$P(r) = \prod_{i}^{N_F} r e^{-rt_i} \prod_{j}^{N_R} e^{-rT_j} \qquad (5)$$

a maximum, where

$r$ is the unknown decay rate,

$t_i$ is the flight time for the _i_th decay in flight (the proper time required for the particle to reach its decay point),

$T_j$ is the moderation time for the _j_th event at rest (the proper time for the _j_th particle to be brought to rest in the emulsion), and

$N_F$ and $N_R$ are the numbers of events in flight and at rest.

The value of the most likely decay rate can be determined by differentiating Eq. (5), and is given by

$$\frac{1}{r} = \frac{1}{N_F}\left[\sum_i^{N_F} t_i + \sum_j^{N_R} T_j\right] . \tag{6}$$

The statistical uncertainty in the value of $r$ is estimated by the expression

$$S(r) = \frac{\left\{\sum_i^{N_F} t_i + \sum_j^{N_R} T_j\right\} - N_F / r}{(N_F)^{1/2}} , \tag{7}$$

which has zero mean and unit variance.[40-42]

If only decays in flight are considered, the appropriate likelihood expression is

$$P(r) = \prod_{i}^{N_F} \frac{re^{-rt_i}}{(1 - e^{-rT_i})}, \tag{8}$$

where

r is the unknown decay rate,
$t_i$ is the flight time for the ith decay, and
$T_i$ is the initial moderation time of the ith decay (the proper time for the particle to come to rest had it not decayed).

By differentiating Eq. (8), the most likely decay rate is found to satisfy the expression

$$\frac{1}{r} = \frac{1}{N_F} \sum_{i}^{N_F} \left( t_i + \frac{T_i}{e^{rT_i} - 1} \right) . \tag{9}$$

The statistical errors are estimated from

$$S(r) = \frac{\sum_{i}^{N_F} \left[ rt_i - 1 + \frac{rT_i e^{-rT_i}}{\left(1 - e^{-rT_i}\right)} \right]}{\left\{ \sum_{i}^{N_F} \left[ 1 - \frac{r^2 T_i^2 e^{-rT_i}}{\left(1 - e^{-rT_i}\right)^2} \right] \right\}^{1/2}}, \tag{10}$$

which also has zero mean and unit variance.[40-42]

## B. Measurements

The data needed to calculate the decay rates are the times which enter the foregoing equations. Moderation times can be obtained from ranges with the aid of tables compiled by Barkas.[29] For the particles that came to rest, the measurement is straightforward. For decays in flight, however, the residual range at the decay point must be determined and added to the measured range to give the initial moderation time. The flight time is the difference between the initial moderation time and the residual moderation time at the decay point.

The residual range of a hyperon that decays in flight can be determined in two ways, either from the energy and laboratory-system angle of emission of the decay product, or from the ionization of the hyperon. In general, decay kinematics fix the hyperon range more accurately than ionization measurements. This is particularly true for $\Sigma^+$ decays by the proton mode. For any decay, however, there are certain angles at which the secondary energy in the laboratory system is insensitive to the velocity of the primary, and for these, ionization measurements often give a more reliable estimate of the residual range. The procedure followed was to calculate the hyperon velocity from the kinematics where possible, and to estimate the error by compounding the errors in angle and energy measurements. If the error was large, ionization measurements were also used and the best value was calculated from the two techniques. A discussion of the ionization measurements is contained in the Appendix.

## C. The $\Sigma^+$ Lifetime Determined by the Proton Decay Mode

A total of 107 $\Sigma^+$ decays into protons found in the A stack have been used to calculate the $\Sigma^+$ decay rate. Of these, 43 were decays in flight and 64 were decays at rest.

Although decays at rest via this mode are easily recognized, decays in flight can simulate proton scatterings if the decay proton is emitted backward in the rest system of the hyperon, but appears emitted forward in the laboratory system. To avoid losing these events, our scanners were instructed to consider every scattering to be a possible $\Sigma^+$ decay; these were later checked for compatibility with the decay mode $\Sigma^+ \rightarrow p + \pi^0$. The final sample of decays in flight was checked for observational bias by calculating the decay angles in the rest system of the hyperon. The distribution of angles was found to be isotropic and therefore no correction for missed events was considered necessary.

The results obtained with these data are shown in Fig. 13, where curve 1 was calculated from Eq. (5), using the 43 decays in flight and the 64 decays at rest, and curve 2 was calculated from Eq. (8), using only the 43 decays in flight. The lifetimes corresponding to the rates at the maxima of these curves are

$$\tau^+ = 0.85^{+0.15}_{-0.11} \times 10^{-10} \text{ sec} \qquad \text{(flight and rest)},$$

$$\tau^+ = 0.86^{+0.75}_{-0.27} \times 10^{-10} \text{ sec} \qquad \text{(flight only)}.$$

The errors were calculated from Eqs. (7) and (10). A graph of Eq. (10) for these data is included in Fig. 14.

All the calculations were performed with an IBM 650.

D. The Hyperon Lifetimes from the Pion Decay Modes

Several difficulties not present in the previous analysis complicate the determination of the decay rates by the pion decay modes. Before the data and results are described, these will be listed. (a) The charge of the hyperon can be determined only if either the decay pion or the pion partner is identified, or if the decay occurs at rest. (b) The $\Sigma^-$ hyperon interacts when it comes to rest. Frequently, however, no star is produced and the hyperon is not recognized. (c) Since the decay at rest of the $\Sigma^+$ hyperon via the pion mode produces a track near the minimum of ionization, the efficiency for detecting these events is less than 100%. (d) The decay kinematics do not determine the

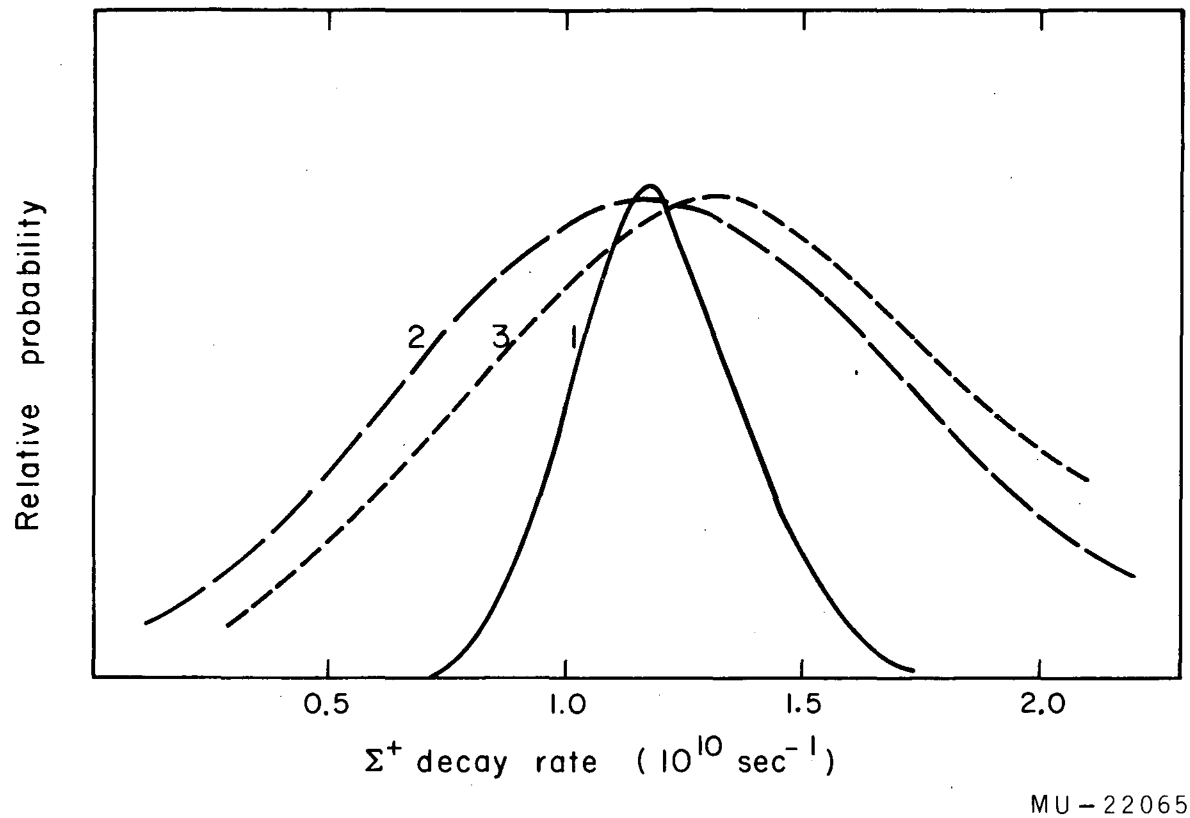


Fig. 13. The relative-likelihood function versus the decay rate for $\Sigma^+$ decays via the proton mode: (1) 64 decays at rest and 43 decays in flight; (2) 43 decays in flight only; and (3) the 43 decays in flight, but with ionization measurements used to determine the $\Sigma$ velocity at its decay point.

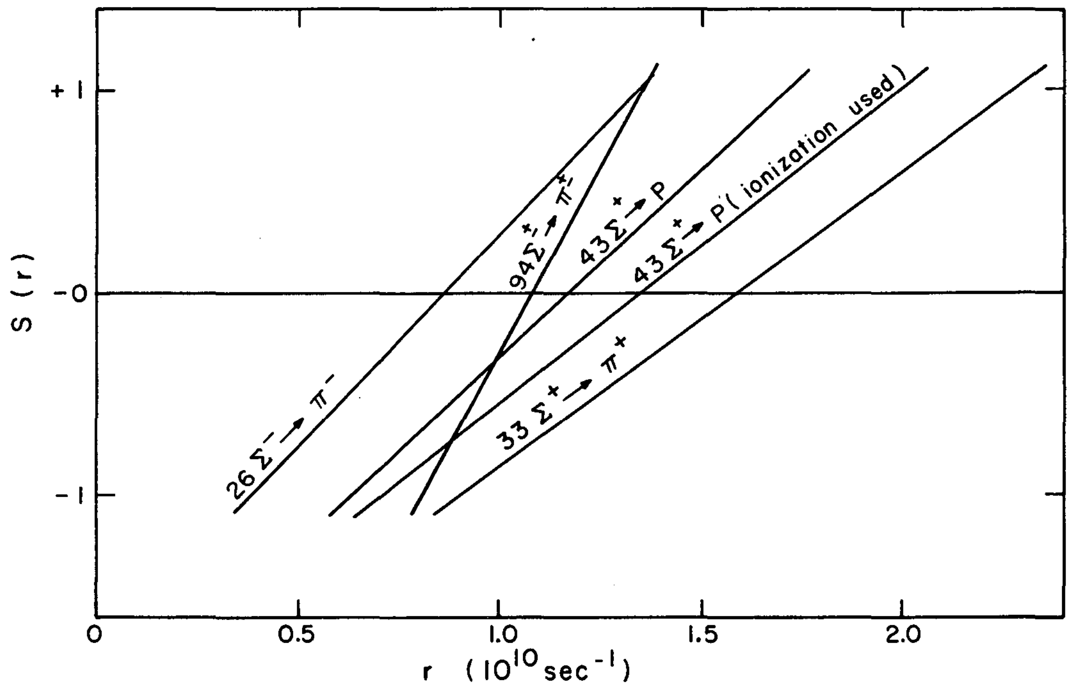


MU-22066

Fig. 14. Plot of S(r) versus r, the decay rate. The values of r for which S(r) is 0 give the most likely rates, and the values of r for which S(r) = ± 1.0 indicate the statistical uncertainty in the most likely rate.

hyperon velocity with accuracy comparable to that obtained with the proton mode; ionization measurements on the hyperon track must more often be relied upon. The residual and flight times at the decays are consequently subject to greater errors than in the case of the proton decay mode of the $\Sigma^+$.

The techniques used to overcome these difficulties are elaborated in the following sections. Two separate analyses of the decay rates have been attempted, one using only the decays in flight, and the other using also the decays and interactions at rest. A list of the hyperons that decay via the pion modes may be found in Table III.

1. The Lifetimes from the Decays in Flight

By using only the decays in flight, the difficulties involved in identifying those hyperons which come to rest can be avoided. In the A stack, 94 such decays were observed, and in 59 cases it was possible to determine the charge of the hyperon by following the decay pion or the pion partner or both. The methods used to effect charge separation are shown in the table below.

| | $\Sigma^-$ | $\Sigma^+$ |
|---|---|---|
| Decay $\pi$ identified | 17 | 8 |
| $\pi$ partner identified | 6 | 14 |
| Both identified | 3 | 11 |
| | 26 | 33 |

The remaining 35 decays could not be identified.

No case was found in which the decay pion and pion partner had the same charge. The reliability of the partner as an indicator of the hyperon charge was further verified by following 27 partners from stars which produced $\Sigma^+ \rightarrow p + \pi^0$ decays. All were negative pions.

Before the lifetime was calculated from these events, some estimate had to be made of the probability of confusing decays at rest with decays that occurred near the end of the hyperon range. The initial separation into "at rest" and "in flight" decays was made when the event was found, and was based upon the appearance of the hyperon

Table III

Summary of Σ hyperons in the A stack

| Type of K Star[a] | $F\Sigma^{\pm}_{\pi}$ | $F\Sigma^{-}_{\pi}$ | $F\Sigma^{+}_{\pi}$ | $F\Sigma^{+}_{p}$ | $R\Sigma^{+}_{\pi}$ | $R\Sigma^{+}_{p}$ | $R\Sigma^{-}_{star}$ | Total |
|---|---|---|---|---|---|---|---|---|
| | Number of Σ hyperons produced[b] | | | | | | | |
| 1 | 5 | 1 | 2 | 7 | 2 | 3 | 7 | 27 |
| 2 | 7 | 4 | 3 | 4 | 3 | 9 | 1 | 31 |
| 2π | 0 | 8 | 17 | 14 | 23 | 30 | 13 | 105 |
| 3 | 14 | 3 | 4 | 6 | 6 | 6 | 7 | 45 |
| 3π | 0 | 3 | 4 | 4 | 10 | 7 | 1 | 30 |
| 4 | 2 | 2 | 1 | 5 | 1 | 5 | 4 | 20 |
| 4π | 0 | 0 | 1 | 0 | 4 | 2 | 3 | 10 |
| 5 | 4 | 1 | 0 | 2 | 1 | 1 | 1 | 10 |
| 5π | 0 | 2 | 1 | 1 | 1 | 1 | 1 | 7 |
| 6 | 1 | 2 | 0 | 0 | 0 | 0 | 1 | 4 |
| 6π | 0 | 0 | 0 | 0 | 0 | 0 | 0 | 0 |
| > 6 | 2 | 0 | 0 | 0 | 0 | 0 | 1 | 3 |
| > 6π | 0 | 0 | 0 | 0 | 0 | 0 | 0 | 0 |
| Total | 35 | 26 | 33 | 43 | 51 | 64 | 40 | 292 |

[a] The numeral indicates the number of star prongs; π indicates that one of the prongs is a π meson.

[b] $F\Sigma^{+}_{\pi}$ indicate $\Sigma^{+} \rightarrow \pi^{+} + n$ in flight, etc.

track. An indication that this judgment was rarely wrong may be had from the following: (a) There were 51 events classed as $\Sigma^+ \rightarrow \pi^+ + n$ at rest. Twenty-three pions from these stopped in emulsion, and all were $\pi^+$ mesons of range compatible with a decay at rest. In addition, 28 partners were identified as $\pi^-$ mesons, and none as $\pi^+$ mesons. (b) None of the 39 pions stopped from the 94 events judged to be decays in flight had ranges compatible with a decay at rest. Therefore, since none of the events which could be checked led to a contradiction of the original classification, it is assumed that errors from this source are negligibly small.

When a sample of decays in flight had been selected and checked, the likelihood function, Eq. (8), was then calculated from the data. Separate curves are shown in Fig. 15 for the $\Sigma^-$ rate determined by the 26 $\Sigma^-$ decays, the $\Sigma^+$ rate determined by the 33 $\Sigma^+$ decays, and a mixed rate determined by combining all 94 decays without distinction as to charge. The lifetimes corresponding to the most likely decay rates are

$$\tau^+ = 0.63^{+0.48}_{-0.19} \times 10^{-10} \text{ sec},$$

$$\tau^- = 1.16^{+1.47}_{-0.43} \times 10^{-10} \text{ sec},$$

$$\tau^\pm = 0.93^{+0.32}_{-0.19} \times 10^{-10} \text{ sec}.$$

The errors are again those calculated from Eq. (10) with the help of Fig. 14.

These estimates indicate shorter values for both the $\Sigma^+$ and $\Sigma^-$ lifetimes than are presently accepted. It appears, however, that a general displacement of the curves of Fig. 15 has occurred; the $\Sigma^-$ lifetime is still approximately twice that of the $\Sigma^+$, and the mixed lifetime is intermediate, as would be expected. The short lifetime calculated from the mixed sample has been observed by other workers in emulsion.[9-19]

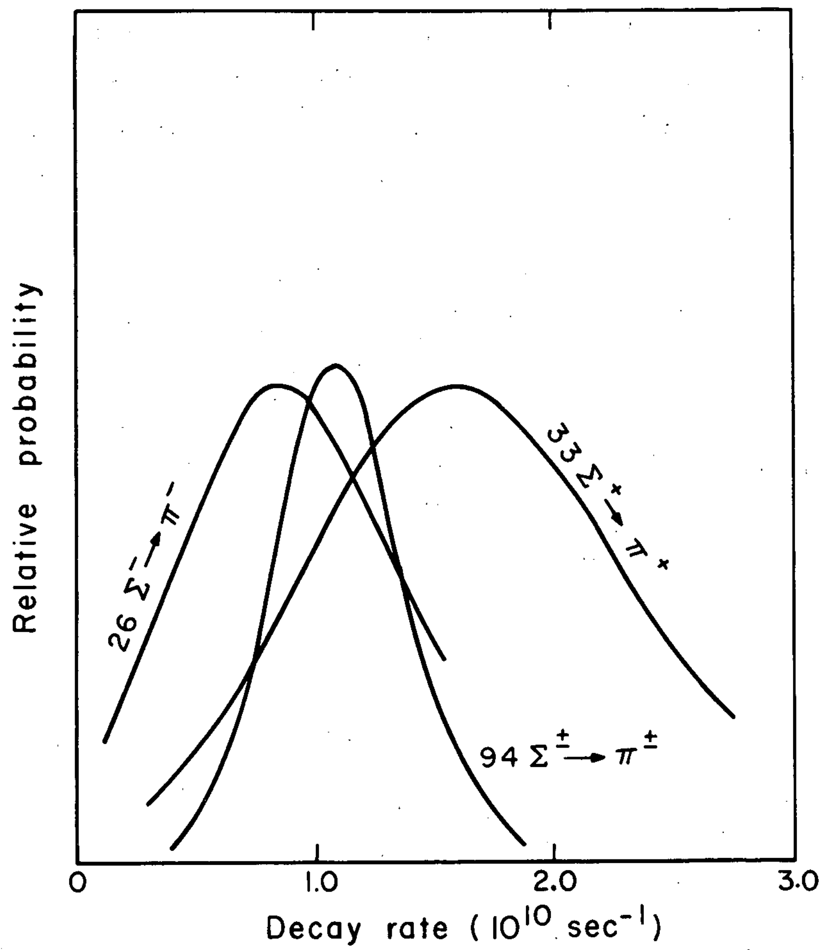


MU-22067

Fig. 15. The relative-likelihood function versus the decay rate for the $\Sigma$ decays in flight via the pion modes. Note that all three of the curves seem to be displaced toward shorter lifetimes than the accepted values.

I believe that the low values of $\tau$ obtained here can be attributed to errors made in estimating the velocities of the hyperons at their decay points. These errors are reflected into the lifetime calculations as errors in the flight and moderation times for each event. From Eqs. (8) and (9) it can be seen that the calculated lifetime depends strongly upon the $T_i$ when they are small compared to $(1/r)$, and becomes relatively insensitive to the $T_i$ when they are large. It is the small values, however, which are subject to the greatest measurement errors, because velocity measurements from ionization become increasingly inaccurate as the velocity decreases. Therefore, the lifetime calculation depends critically upon just those measurements that are the most uncertain.

It is clear that systematic errors in the velocity estimates alter the results of the lifetime calculation; for example, if the velocities are all increased, the $T_i$ increase and the $t_i$ decrease, both tending to lower the lifetime. That random errors in velocity also alter the mean value of the decay rate calculated from Eq. (8) or (9) can be seen from the form of these expressions; the moderation times $T_i$ do not enter linearly into them.

To show that random errors operate to lower the apparent lifetime, a test was made on those $\Sigma^+$ decays by the proton mode which had already been used to establish a satisfactory $\Sigma^+$ lifetime including only decays in flight. For 25 of the 43 events, velocities obtained from the decay kinematics were discarded and replaced by velocities estimated by ionization measurements. Only 25 events were selected because this number represents about the same percentage of the sample as was treated by ionization measurements in the pion decay modes. The remaining events are either too steep or too short for such measurements. In Fig. 24 in the Appendix the two estimates of the velocity for each event are compared. The mean value for all 25 decays is $\beta = 0.213$ by ionization and $\beta = 0.212$ by kinematics; the errors are apparently random. By using the ionization measurements, new values for the flight and moderation times were calculated for each of the 25 events. The remaining 18 events were unaltered.

The curves of P(r) and S(r) from all 43 decays — but with data from ionization used in 25 cases — were then calculated as before, and are shown in Figs. 13 and 14. The lifetime corresponding to the most likely decay rate is now

$$\tau^{+} = 0.74^{+0.63}_{-0.25} \times 10^{-10} \text{ sec} .$$

The lifetime has indeed been lowered somewhat. That the value from the pion decay mode is even smaller can probably be attributed to the fact that the entire sample of $\Sigma^{+} \rightarrow \pi^{+} + n$ decays is subject to relatively large errors even when kinematic analysis is used, while only a portion of the present sample is so affected.

Similar conclusions have been reached by Freden et al.[18] who introduced errors into a group of $\Sigma^{+} \rightarrow p + \pi^{0}$ decays by changing the hyperon energies by ± 20%. Increasing the energies of half of the sample and decreasing the remainder simulates random errors; they found that such an altered group of decays leads to a lifetime almost two standard deviations smaller than that obtained from their unaltered data.

It appears, then, that lifetimes calculated from Eqs. (8) and (9) are subject to severe biases arising from random errors in the input data, and give accurate estimates only if the input errors are small. For the pion decay modes of the hyperons considered here, the errors are not small, and therefore the calculated lifetimes should be regarded as lower limits.

## 2. Lifetime Estimates with Events at Rest Included

According to Eq. (5), if the sample of particles whose lifetime is to be determined includes events at rest, the initial moderation times for the decays in flight do not enter explicitly into the calculations. Because the latter are presumably to blame for the low values of $\tau$ already calculated from the decays in flight alone, this second analysis was undertaken. It might appear that this amounts to trading one sort of trouble for another — now that estimates of the true number of events at rest must be made -- but it will be shown that these do not introduce large errors.

Because there are decays in flight whose charge is not known, no complete sample of events can be selected for either the $\Sigma^+$ or $\Sigma^-$ lifetime calculation. Instead, a joint likelihood function can be constructed which includes particles of both charges and allows for two different lifetimes.

If $x$ is the $\Sigma^+$ decay rate and $y$ is the $\Sigma^-$ decay rate, then we have

$$P(x, y) = \prod_j^{N_{R+}} e^{-xT_j} \prod_k^{N_{R-}} e^{-yT_k} \prod_i^{N_F} \left[ P_i x e^{-xt_i} + (1-P_i) y e^{-yt_i} \right], \quad (11)$$

where the first product is over the $\Sigma^+$ decays at rest, the second over the $\Sigma^-$ interactions at rest, and the third over the decays in flight.[16] $P_i$ is defined as the probability that the ith decay in flight be a $\Sigma^+$. If every decay in flight were of known charge ($P = 0$ or $1$), Eq. (11) would be simply the product of Eq. (5) taken for the $\Sigma^+$ and $\Sigma^-$ cases separately; also the most likely decay rates, $x$ and $y$, would be independent.

Equation (11) can be solved to give the most likely rates,

$$\frac{1}{x} = \frac{\sum_j^{N_{R+}} T_j + \sum_m^{N_{F+}} t_m}{N_{F+}} - \frac{1}{N_{F+}} \sum_i^{N_{F\pm}} \frac{P_i e^{-xt_i} (1 - xt_i)}{P_i x e^{-xt_i} + (1-P_i) y e^{-yt_i}} \quad (12)$$

and

$$\frac{1}{y} = \frac{\sum_{k}^{N_R -} T_k + \sum_{n}^{N_F -} t_n}{N_F -} - \frac{1}{N_F -} \sum_{i}^{N_F \pm} \frac{(1-P_i)\, e^{-yt_i} (1 - yt_i)}{P_i\, xe^{-xt_i} + (1-P_i)\, ye^{-yt_i}} , \tag{13}$$

where $N_F+$ and $N_F-$ are the numbers of decays in flight of known charge, and $N_F\pm$ is the number of decays in flight of unknown charge. For $N_F\pm = 0$, the two decay rates are independent and these equations reduce to Eq. (6).

Before these equations could be used, the $P_i$ and the total moderation times for the events at rest had to be calculated. The techniques used for determining these will be discussed before the results of the calculations are presented.

(a) Estimation of the $P_i$

There are 35 decays of unknown charge. To estimate the $P_i$, these have been separated into three groups, as follows:

Group I: $\Sigma$ energy $>60$ Mev, and no $\pi$ partner

When my data were combined with those of the $K^-$ Collaboration experiment,[35] 10 $\Sigma^+$ and 16 $\Sigma^-$ were identified among particles belonging to this group. Three of the $\Sigma^+$ and 13 of the $\Sigma^-$ are accompanied by a proton partner of energy $\geq 30$ Mev. Thus, if such a fast proton partner is observed, we have $P_i = 0.27$; if not, $P_i = 0.79$. This group contains 19 of the unknown decays.

Group II: $\Sigma$ energy $>60$ Mev, and no other star prong

Five $\Sigma^+$ and no $\Sigma^-$ have been identified in this group. $P_i$ is therefore 1.0. This group contains only one of the unknown decays.

Group III: $\Sigma$ energy $< 60$ Mev, and no $\pi$ partner

The $P_i$ in this group are estimated by comparing with $\Sigma^+$ decays via the proton mode which belong to the same group. There are 23 of these at rest and 19 in flight. If we now assume that the ratio rest/flight is the same for $\Sigma^+$ decays via the pion mode in this group, the expected number of $\Sigma^+$ decays in flight can be gotten from the observed number of $\Sigma^+$ decays at rest. There are 18 $\Sigma^+ \rightarrow \pi^+$ at rest; therefore there should be 15 $\Sigma^+ \rightarrow \pi^+$ in flight. There are 24 decays in flight, thus $P_i = 15/24 = 0.62$. This group contains the remaining 15 of the unknown decays.

There are no decays of unknown charge accompanied by a $\pi$ partner.

(b) Estimation of the Total $\Sigma^-$ Moderation Time

A large fraction of these particles interact at rest without producing any clue as to their identity. The total moderation time for all $\Sigma^-$ hyperons must therefore be estimated from the fraction of these which do produce recognizable stars in the emulsion.

The collinear events furnish a sample of $\Sigma^-$ hyperons whose terminal behavior can be studied to form an estimate of the number of events that would normally escape detection. By combining data with those reported by the $K^-$ Collaboration experiment,[35] a sample of 95 $\Sigma^-$ endings is obtained. These are divided into recognizable and nonrecognizable terminations as follows: A termination is considered recognizable if a star is produced which has more than 1 prong, or if it has 1 prong of $\geqslant 200\ \mu$ range; otherwise, a termination is considered nonrecognizable. With these criteria, 30 recognizable stars are observed among the 95 $\Sigma^-$ endings. The ratio of all $\Sigma^-$ endings to recognizable $\Sigma^-$ endings is therefore $95/30 = 3.17 \pm 0.48$.

In the A stack, 40 star prongs were observed to terminate with the production of a recognizable star, and are presumably $\Sigma^-$ interactions at rest. To further verify this identification — and to check for the presence of singly-charged hyperfragments — the $\pi$ partners were followed whenever they existed. Only 18 of the $K^-$ stars produced a $\pi$ partner; 15 of these were followed to rest and identified as $\pi^+$ mesons. The remaining 3 could not be identified.

Assuming that these 40 prongs represent the recognizable $\Sigma^-$ terminations in the A stack, the total $\Sigma^-$ moderation time is estimated by multiplying the moderation time for these events by the factor $3.17 \pm 0.48$, which gives $(43.49 \pm 6.59) \times 10^{-10}$ sec. To this must be added the moderation time for the 9 $\Sigma^-$ produced in collinear events in the A stack, giving finally $(45.57 \pm 6.59) \times 10^{-10}$ second, the figure used in the lifetime calculations.

(c) Estimation of the Total $\Sigma^+$ Moderation Time

In principle, this is well known from the ranges of the 51 observed $\Sigma^+ \rightarrow \pi^+ + n$ decays at rest, but some correction must be made for the observational loss of these events. Past experience indicates that this loss is apt to be a function of the dip angle of the emitted pion, and of the depth in emulsion at which the decay occurs.

To check for the first bias, the distribution of sin $\delta$ was investigated; equal intervals of sin $\delta$ should be equally populated. When divided into 10 intervals, the distribution appears as in Fig. 16. The $\chi^2$ test applied to this distribution indicates a probability of 0.2 that larger deviations would be found in another experiment.

To check for the second bias, the position of each decay— the height measured from the emulsion-glass interface divided by the pellicle thickness— was measured. The decays should, of course, be randomly distributed. This distribution is also shown in Fig. 16, and the $\chi^2$ test applied to it gives a probability 0.4 that larger deviations would be found in another experiment.

No reasonable corrections to the observed number of decays can be made on the basis of these distributions. This unusually low loss factor is the fruit of very careful inspection of each prong termination by a group of experienced scanners working with emulsion relatively free from distracting background tracks. It is not reasonable, however, that the loss should be zero, particularly for those decays which occur quite close to a pellicle surface. Upon further division, the distribution of decays according to depth in emulsion

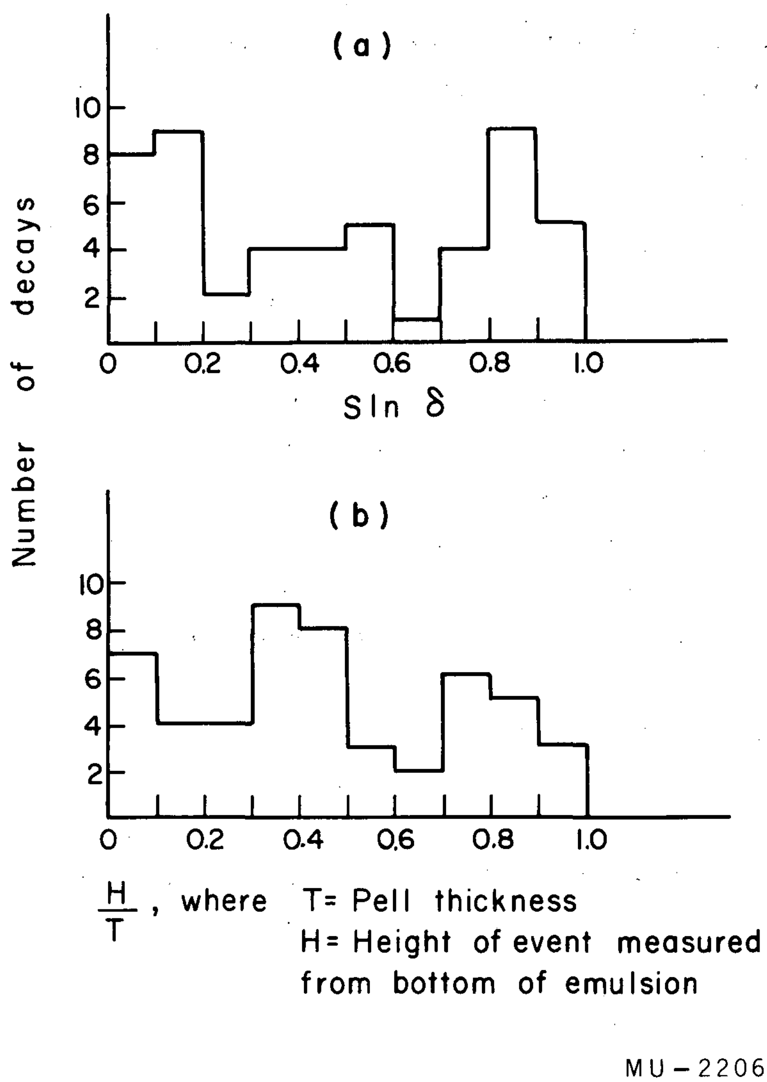


Fig. 16. Tests for biases in observation loss of $\pi$ mesons from $\Sigma^+ \rightarrow \pi^+ + n$ decays at rest: (a) shows the number of decays observed vs the sine of the dip angle; and (b) shows the number of decays observed vs the position of the decay, i.e., the depth in emulsion at which the decay occurs. These plots show no significant biases.

shows that there is only one decay within 15 μ of either surface. There should be five. Consequently, based on this evidence alone, the number of $\Sigma^+ \rightarrow \pi^+ + n$ decays at rest has been increased from 51 to 55 and the total moderation time increased correspondingly.

(d) Calculation of the Lifetimes

Eqs. (12) and (13) were solved on the IBM 650. Using the best estimates outlined above for the quantities involved, the most likely lifetimes were found to be $\tau^+ = 0.80 \times 10^{-10}$ sec and $\tau^- = 1.75 \times 10^{-10}$ sec.

Errors introduced into the calculated lifetimes by errors associated with the input data were determined as follows: (a) The effect of the uncertainties in the total moderation times was calculated directly by altering these times by one standard deviation and re-calculating the lifetimes. Four separate recalculations were involved. (b) To estimate the sensitivity of the result to changes in the $P_i$, these were all set equal to 0.5 and the lifetimes were again recalculated.

The statistical error to associate with each lifetime was determined by plotting the likelihood function of Eq. (11), first as a function of x with y fixed at its most likely value, and then as a function of y with x fixed at its most likely value. These curves are shown in Fig. 17. The spread of the curves at 60% height was taken as the statistical uncertainty. The same result was obtained from Eq. (10) when the total number of $\Sigma^+$ and $\Sigma^-$ decays in the unknown group was estimated from the $P_i$.

The uncertainties introduced into the lifetimes from these sources are listed below.

| Error | $\Delta\tau^+ \times 10^{-10}$ sec | $\Delta\tau^- \times 10^{-10}$ sec |
|---|---|---|
| $\Sigma^-$ moderation time | ±0.005 | ±0.19 |
| $\Sigma^+$ moderation time | ±0.02 | negligible |
| $P_i$ | 0.02 | 0.02 |
| statistical | +0.13, -0.10 | +0.34, -0.24 |

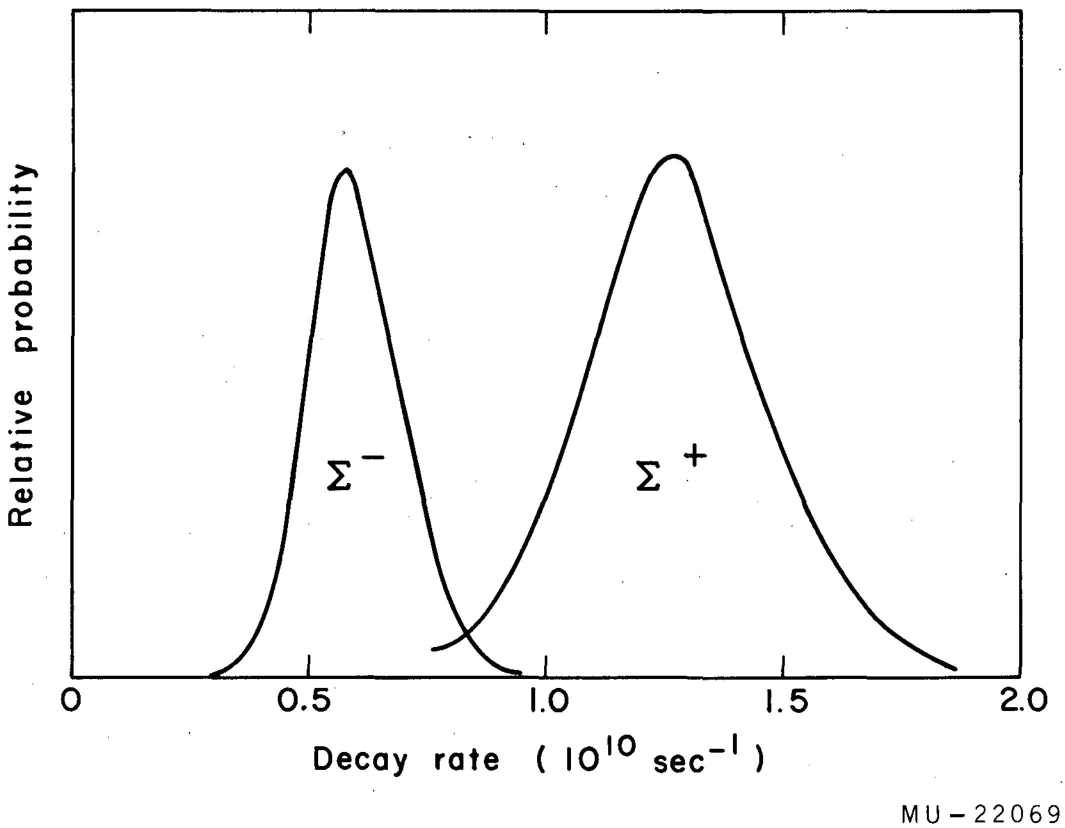


Fig. 17. The joint-likelihood function vs the decay rate. The curve for $\Sigma^-$ is plotted with the $\Sigma^+$ decay rate held constant at its most likely value, and vice versa.

The best estimates of the lifetimes, and their errors, are then

$$\tau^{+} = 0.80^{+0.14}_{-0.11} \times 10^{-10} \text{ sec and}$$

$$\tau = 1.75^{+0.39}_{-0.30} \times 10^{-10} \text{ sec ,}$$

which are in good agreement with other published values.[7,8]

Finally, by combining the data from both decay modes of the $\Sigma^{+}$, the best estimate of the $\Sigma^{+}$ lifetime becomes

$$\tau^{+} = 0.82^{+0.10}_{-0.08} \times 10^{-10} \text{ sec.}$$

E. Summary and Discussion of Data

Several emulsion groups have measured the $\Sigma^{+}$ lifetime by analysis of the proton decay mode. The two most recent published values are $0.85^{+0.14}_{-0.11} \times 10^{-10}$ sec, by Freden et al.[18] using 117 decays, and $0.82^{+0.34}_{-0.20} \times 10^{-10}$ sec, by Evans et al.[17] using 41 decays. The best value from bubble-chamber data is $(0.75 \pm 0.1) \times 10^{-10}$ sec.[8] These values are consistent.

Emulsion measurements on the pion decay modes have, however, consistently yielded low values for the lifetime. Generally, it has not been possible to separate $\Sigma^{+}$ and $\Sigma^{-}$ decays for separate analysis, owing to the long ranges of the decay pions and pion partners. Some of the published data are listed below.

| Lifetime (x $10^{-10}$ sec) | Data | Reference |
|---|---|---|
| $\tau^{\pm} = 0.38^{+0.10}_{-0.06}$ | 41 $\Sigma^{\pm}$ in flight | 10 |
| $\tau^{\pm} = 0.31^{+0.32}_{-0.10}$ | 6 $\Sigma^{\pm}$ in flight | 11 |
| $\tau^{\pm} = 0.35^{+0.15}_{-0.11}$ | 11 $\Sigma^{\pm}$ in flight | 12 |

| Lifetime (x $10^{-10}$ sec | Data | Reference |
|---|---|---|
| $\tau^{\pm} = 0.32^{+0.11}_{-0.07}$ | 26 $\Sigma^{\pm}$ in flight | 13 |
| $\tau^{\pm} = 0.7^{+0.19}_{-0.16}$ | 24 $\Sigma^{\pm}$ in flight | 15 |
| $\tau^{\pm} = 0.71^{+0.19}_{-0.12}$ | 70 $\Sigma^{\pm}$ in flight | 17 |
| $\tau^{\pm} = 0.66^{+0.14}_{-0.13}$ | 162 $\Sigma^{\pm}$ in flight | 19 |
| $\tau^{\pm} = 0.93^{+0.32}_{-0.19}$ | 94 $\Sigma^{\pm}$ in flight | this experiment |

There is very little information available on the pion decay modes where the hyperon charge is known. Freden et al. report $\tau^{+} = 0.60^{+0.68}_{-0.20} \times 10^{-10}$ sec, based on 37 $\Sigma^{+}$ decays in flight via the pion mode. The value obtained in this paper is $\tau^{+} = 0.63^{+0.48}_{-0.19} \times 10^{-10}$ sec, based on 33 decays. There are no published data on the $\Sigma^{-}$ lifetime determined from decays in flight. The value, $\tau^{-} = 1.16^{+1.47}_{-0.43} \times 10^{-10}$ sec, reported in this paper is the first such determination.

As discussed earlier in the text, the low values obtained even when charge separation can be effected indicate that measurements on the pion decay modes probably produce biased lifetime estimates. There is no need to introduce an unknown particle of short lifetime to explain the data.

Other estimates of the $\Sigma^{-}$ lifetime in emulsion have been hampered by a lack of data indicating the proper assignment of charge for decays in flight and large uncertainties concerning the number of $\Sigma^{-}$ interactions at rest. The two best values previously available are $\tau^{-} = 1.65 \times 10^{-10}$ sec, by Evans et al.,[17] and $\tau^{-} = 1.7^{+1.1}_{-0.5} \times 10^{-10}$ sec by Giles.[23] The value reported in this paper represents a considerable statistical improvement because much more information is available concerning the charges of the hyperons and the number of $\Sigma^{-}$ interactions. My estimate is $\tau^{-} = 1.75^{+0.39}_{-0.30} \times 10^{-10}$ sec.

In summary, recent data indicate that there is no longer any real discrepancy between bubble-chamber and emulsion estimates of the $\Sigma$ lifetimes. The low values obtained for decays in flight via the pion modes in emulsion can be attributed to errors in the measurements and do not necessitate the introduction of a new particle.

## V. BRANCHING RATIOS

### A. The Branching Ratio $\frac{(\Sigma^+ \rightarrow p + \pi^o)}{\text{all } \Sigma^+}$

As mentioned before, 107 $\Sigma^+$ decays into protons have been observed in the A stack, and the efficiency for detecting these has been taken to be 100%. The total number of $\Sigma^+$ decays into $\pi^+$ mesons can now be calculated as follows: (a) There are 51 decays at rest and 33 decays in flight known to be $\Sigma^+ \rightarrow n + \pi^+$. (b) There are 35 decays in flight into pions of unknown charge. The number of $\Sigma^+ \rightarrow n + \pi^+$ represented by this group is estimated to be $\Sigma\ P_i = 17$. (c) It has been estimated that four decays at rest were lost by failure to observe the pion. By combining these numbers, the total number of $\Sigma^+ \rightarrow n + \pi^+$ is 105.

The branching ratio therefore is

$$\frac{\Sigma^+ \rightarrow p + \pi^o}{\text{all } \Sigma^+ \text{ decays}} = \frac{107}{212} = 0.50 \pm 0.03 ,$$

which agrees with recent values from both bubble-chamber and emulsion groups.[18, 22]

### B. The Branching Ratio $\frac{\Sigma^+ \rightarrow p + \gamma}{\Sigma^+ \rightarrow p + \pi^o}$

The decay mode $\Sigma^+ \rightarrow p + \gamma$ occurring at rest would produce a proton of 26.5 Mev energy and 3.0 mm range in emulsion. There is no such candidate among the 95 decays at rest via the proton mode in the A, 2B, and 1U stacks. There is, however, the possibility of confusing such a decay with a decay by the normal proton mode occurring slightly in flight; for example, a $\Sigma^+$ with 100 $\mu$ residual range will emit a proton of 3.0 mm range if the decay angle is approximately 50 deg. An event such as this would be classed "in flight" on the basis of the proton range, even though it might not be clear from the hyperon track itself that the decay did not occur at rest. To check this possibility, the proton ranges from the $\Sigma^+ \rightarrow p$ decays in flight in the A and 2B stacks have been plotted in Fig. 18. There is no evidence of grouping around 3 mm, but there are two ranges very close to the expected value from $\Sigma^+ \rightarrow p + \gamma$. The actual measured ranges are 3043 $\mu$ and 3047 $\mu$. Neither one of these represents a possible case of $\Sigma^+ \rightarrow p + \gamma$ decay, however; in one case the hyperon residual range at the decay point is 2.2 mm, and in the other case it is 1.3 mm. Ionization measurements and kinematic analysis on the assumption that the decays are via the normal proton mode give consistent results. Since these are the only two cases whose proton range is within straggling errors of 3 mm, it is concluded that there are no $\Sigma^+ \rightarrow p + \gamma$ decays at rest erroneously classed as $\Sigma^+ \rightarrow p + \pi^0$ decays in flight.

An upper limit can be put on the branching ratio on the basis of the 95 decays at rest:

$$\frac{\Sigma^+ \rightarrow p + \gamma}{\Sigma^+ \rightarrow p + \pi^o} = \frac{0}{95} \text{ observed.}$$

Two other groups have observed a total of zero $\Sigma \rightarrow p + \gamma$ decays among 138 $\Sigma^+ \rightarrow p + \pi^o$ decays.[18, 43] Quareni et al., however, have reported three possible $\Sigma^+ \rightarrow p + \gamma$ decays and estimate the branching ratio to be approx 1%.

Theoretical predictions for this branching ratio range from 0.01% to 1.0%.[45]

C. The Branching Ratio for Leptonic Decays

Although theoretical predictions based on the assumption of a universal Fermi interaction indicate that a few percent of all hyperon decays should proceed with the production of leptons, experimental data indicate that these decays are virtually absent. Only two leptonic decays have been observed, both examples of $\Lambda \rightarrow e^- + p + \bar{\nu}$. The figures recently collected by Glaser summarize the situation:[19]

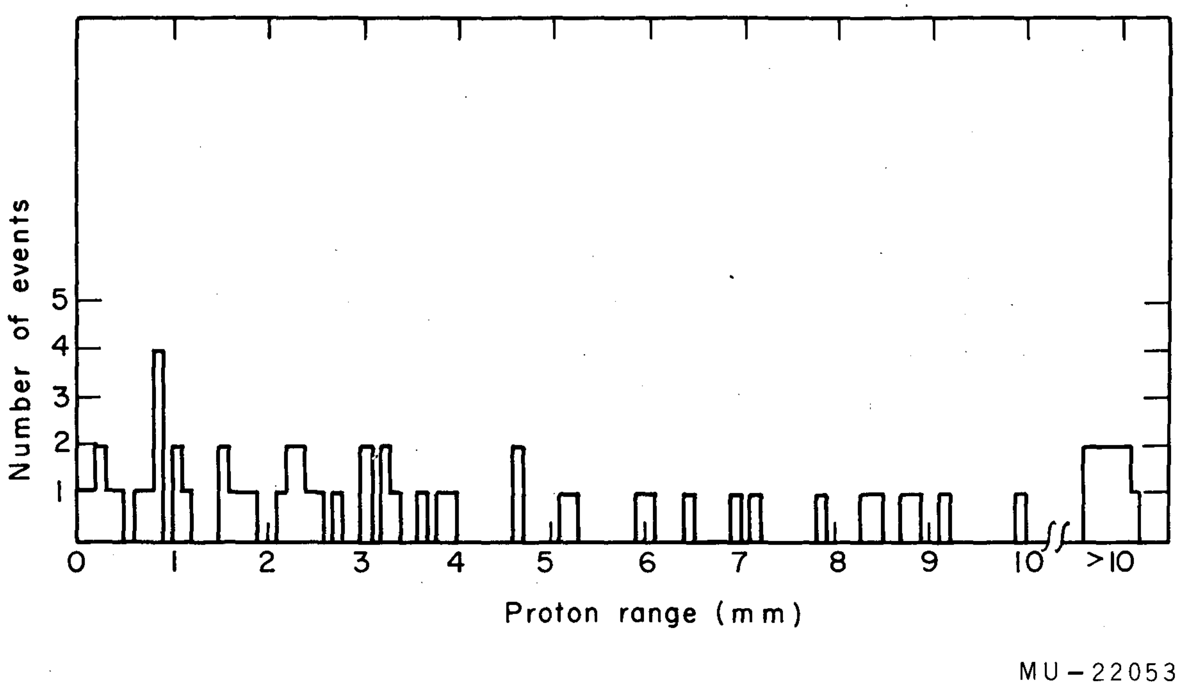


Fig. 18. Proton ranges from $\Sigma^+ \to p + \pi^o$ decays in flight in the A and 2B stacks.

| Mode | Experimental limit | Prediction |
|---|---|---|
| $\Lambda \rightarrow e^- + p + \overline{\nu}$ | 0.2% | 1.6% |
| $\Lambda \rightarrow \mu^- + p + \overline{\nu}$ | 0.1 | 0.24 |
| $\Sigma^- \rightarrow e^- + n + \overline{\nu}$ | 0.2 | 5.8 |
| $\Sigma^- \rightarrow \mu^- + n + \overline{\nu}$ | 0.2 | 2.5 |
| $\Sigma^+ \rightarrow e^+ + n + \nu$ | 0.3 | --- |
| $\Sigma^+ \rightarrow \mu^+ + n + \nu$ | 0.3 | --- |

Experiment and theory are strikingly at variance in the case of the $\Sigma^-$.

Despite the fact that the number of decays already observed—mostly in bubble-chamber groups — far exceeds the number gathered for this experiment, evidence for leptonic decays was sought among the events in the 2B and A stacks.

To separate such decays in emulsion from the normal pion decay modes, it is necessary to follow the decay product and attempt to identify it. In all, 196 near-minimum tracks from $\Sigma$ decays were followed, with the results listed below:

| Secondary fate | From $\Sigma$ at rest | From $\Sigma$ in flight |
|---|---|---|
| $\pi^+$ to rest in emulsion | 25 | 29 |
| $\pi^-$ to rest in emulsion | 0 | 23 |
| $\pi^\pm$ interacts in flight | 8 | 21 |
| secondary leaves stack | 29 | 61 |
| | 62 | 134 |

In 90 cases the secondary leaves the emulsion stacks and is therefore not identified. An argument that these are all pions, however, can be based upon the following observations: (a) Average path length for these particles is approx 70 mm, and only three of them are less than 50 mm. Most of them undergo sufficient change in ionization before leaving the stack to indicate compatibility with the decay modes $\Sigma \rightarrow \pi + n$. (b) Since the average path length is about 2.5 times the radiation length in emulsion, it is highly unlikely that an electron would escape without sufficient reduction in energy to make its identification by scattering obvious. (c) Muons from the leptonic decays would be produced with a spectrum of energies. From $\Sigma^-$, about 80% of these should have ranges less than 8 cm in emulsion. The chance that a muon would be produced at such an energy and angle that its change of ionization would indicate compatibility with a pion decay mode is small. (d) There are no leptons among the 106 identified secondaries.

In all, a total of 11.5 meters of secondary track from $\Sigma$ decays was followed and no behavior atypical of pions was observed.

There are 105 $\Sigma^+$ decays, 38 $\Sigma^-$ decays, and 53 $\Sigma^\pm$ decays among the 196 events. By use of the $P_i$ defined before, the 53 $\Sigma^\pm$ decays are estimated to contain 24 $\Sigma^+$ hyperons and 29 $\Sigma^-$ hyperons; therefore, 129 $\Sigma^+$ decays and 67 $\Sigma^-$ decays are in the sample.

Estimating the number of leptonic decays to be zero unables one to set rough upper limits,

$$\frac{\Sigma^+ \rightarrow \text{leptons}}{\Sigma^+ \rightarrow \pi^+} = \frac{0}{129}, \quad \text{and}$$

$$\frac{\Sigma^- \rightarrow \text{leptons}}{\Sigma^- \rightarrow \pi^-} = \frac{0}{67}.$$

The collected data, including those above, now total over 500 $\Sigma^-$ decays and nearly 400 $\Sigma^+$ decays in which leptonic modes could have been detected.[46] No such decay has yet been observed.

# APPENDIX: IONIZATION MEASUREMENTS

Measurements of ionization as a function of particle velocity in the region $\beta \approx 0$ to $\beta \approx 0.5$ were undertaken in the A stack to aid in the lifetime studies. These measurements were often the only method by which the hyperon moderation and flight times could be determined.

## Theory

Barkas has recently derived a rather complete statistical theory of track structure in emulsion and has been able to show connections between several observable functions of the ionization.[47] Some important results of this theory are reviewed here.

The ionization caused by a particle as it passes through the emulsion is revealed by the formation of "grains" in the developed track. The density of grains – their number per unit length – is a function of particle velocity, but is not directly observable because they coalesce to form "blobs." A track therefore appears as a succession of blobs separated by gaps of varying lengths. It is the density and distribution of these that are the observable features of track structure which may be related to particle velocity.

The gap-length distribution is exponential,

$$H(x) = Be^{-gx}, \qquad (14)$$

where $H(x)$ = the density of gaps of length exceeding $x$;

$B$ = the density of gaps of length exceeding zero, or the blob density; and

$g$ = the true grain density.

The blob density is related to the grain density by

$$B = ge^{-g\alpha}, \qquad (15)$$

where $\alpha$ is the mean distance between centers of "just resolvable" grains; in the limit of perfect resolution it becomes the mean grain diameter. The value of $\alpha$ can be determined for any observational conditions by noting that $B$ passes through a maximum, $B_{max} = 1/(e\alpha)$, when $g$ has the value $g = 1/\alpha$. By counting $B_{max}$, the value of $\alpha$ appropriate for a particular observer and optical system can be determined. The linear fraction of track occupied by gaps is given by $L = e^{-g\alpha}$ and is defined as the track lacunarity. Three indirect measures of $g$ are suggested by these relations:

$$g = (1/x) \ln (B/H(x)) = (1/\alpha) \ln (1/L) = B/L .$$

In addition, the quantities $B$ and $L$ themselves can be determined as functions of particle velocity.

To be useful, these formulas must be extended to include measurements made on tracks which are inclined to the emulsion surface. If $\delta$ is the dip angle in unprocessed emulsion — $\delta = 0$ for tracks parallel to the emulsion surface — then Eqs. (14) and (15) become

$$H_\delta(x) = B_\delta \, e^{-gx \sec \delta} \quad \text{and} \tag{16}$$

$$B_\delta = g \sec \delta \; e^{-\alpha g \sec \delta} , \tag{17}$$

where the subscripts $\delta$ indicate quantities measured per unit projected length when the dip angle is $\delta$. From Eq. (17) a universal curve for $\alpha B_\delta$ versus $\alpha g \sec \delta$ can be constructed, and is shown in Fig. 19.

The track lacunarity measured for a dipping track becomes

$$L_\delta = e^{-g\alpha \sec \delta} = L \, e^{-g\alpha (\sec \delta - 1)} .$$

The relation between $L$ and $L_\delta$ is plotted in Fig. 23.

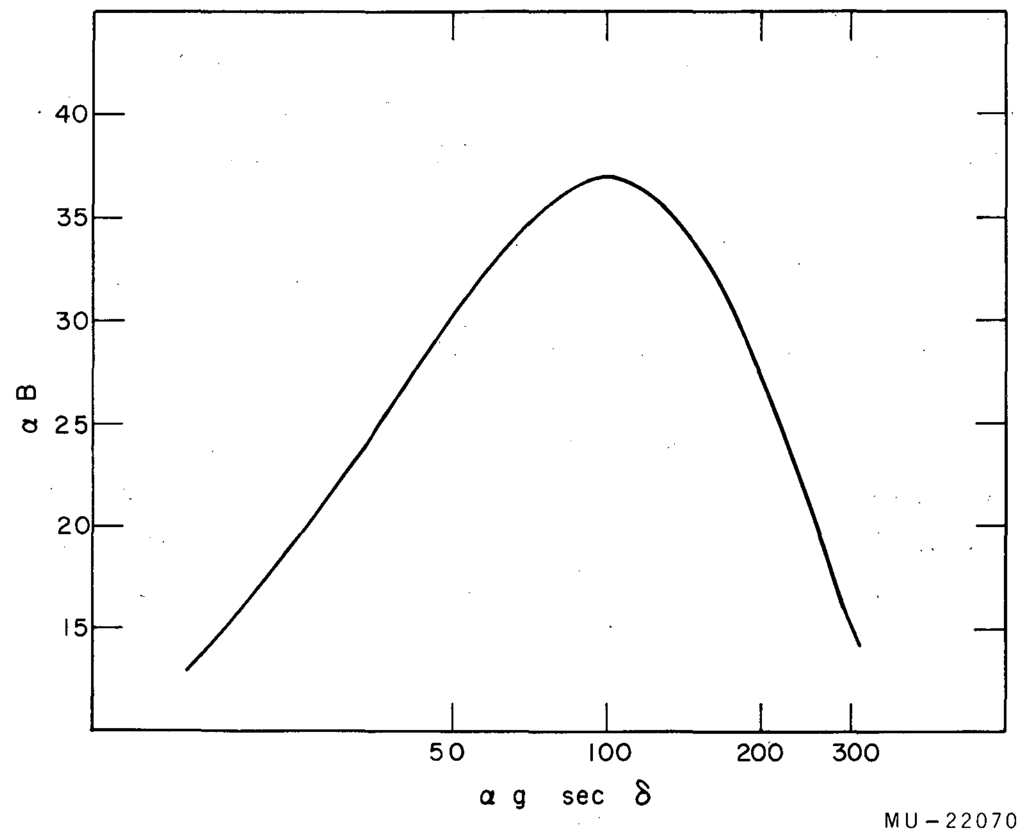


Fig. 19. The relation $\alpha B = \alpha g \sec \delta \; e^{-\alpha g \sec \delta}$, with $\alpha B$ plotted against $\alpha g \sec \delta$. The quantities are defined in the text.

Finally, the relations between g and the observed quantities become

$$g = \frac{\cos\delta}{x} \ln \frac{B_\delta}{H_\delta(x)} ,$$

$$g = \frac{\cos\delta}{a} \ln \frac{1}{L_\delta} , \text{ and}$$

$$g = \cos\delta \, (B_\delta / L_\delta) .$$

These corrections for inclined tracks are not exact, but for dip angles up to about 60 deg they differ by a negligible amount from the exact formulas.

## Equipment Used

All measurements were performed with an automated microscope and recording system recently designed for ionization measurements,[35] consisting fundamentally of the following:

(a) A microscope with a motor-driven stage, whose speed is controlled by the observer. The track being studied is caused to pass under a hairline in the microscope eyepiece at some convenient rate.

(b) A switch, similar to a telegraph key, which is held down when a gap (or blob) is under the hairline.

(c) Automatic recording devices which simultaneously register the total length of track which has passed under the hairline, the total number of gaps, the integrated gap length, and the number of gaps which exceed each of 10 preset lengths ranging from 0.5 μ to 10 μ.

The quantities B, L, and H(x) are thus all determined by a single traversal of a track segment.

## Measurements

The velocities of most of the hyperons that decayed in flight were in the region $\beta \approx 0.1$ to $\beta \approx 0.35$. In this region the blob density passes through its maximum ($\beta \approx 0.25$) and is consequently a relatively insensitive measure of ionization. The true grain density is difficult to establish from the formula $g = (1/x) \ln [B/H(x)]$ in this region because of the errors involved in measuring $H(x)$ when $x$ is very small. Therefore, it was decided that $L$ and $g \approx B/L$ would be used to estimate $\beta$, and curves of these quantities versus velocity were constructed.

The first step in this program was to measure $B$ as a function of residual range for five flat $K^-$ tracks ($\delta \approx 0$ deg) in order to establish $B_{max}$ and $\alpha$ for the equipment used. The results of this counting are plotted in Fig. 20. To test for variations of $B_{max}$ in different pellicles, the $K^-$ tracks were selected from various parts of the stack; no more than statistical differences were found. The maximum of the curve of Fig. 20 gives $B_{max} = 63$ blobs/100 $\mu$, and therefore $\alpha = 0.58\ \mu$. This value of $\alpha$ was later used to make the corrections in lacunarity for inclined tracks according to the curves of Fig. 23.

The curves of $B/L$ and $L$ versus $\beta$ were first established by using the same five $K^-$ tracks, and are represented by the solid lines of Figs. 21 and 22.

Finally, the validity of the correction for dip angle and the correctness of the curves for tracks other than the five $K^-$ mesons were checked by measuring several protons of known velocity and various dip angles. The lacunarity correction of Fig. 23 was used. Points obtained from these tracks are shown on Figs. 21 and 22.

These data indicate that the curves are accurate and should provide reliable estimates of hyperon velocities. The crucial test, of course, is to apply ionization measurements to hyperons of known velocity. The $\Sigma^+ \rightarrow p + \pi^0$ decays in flight provide a convenient sample of these and the results obtained with 25 tracks are shown in Fig. 24.

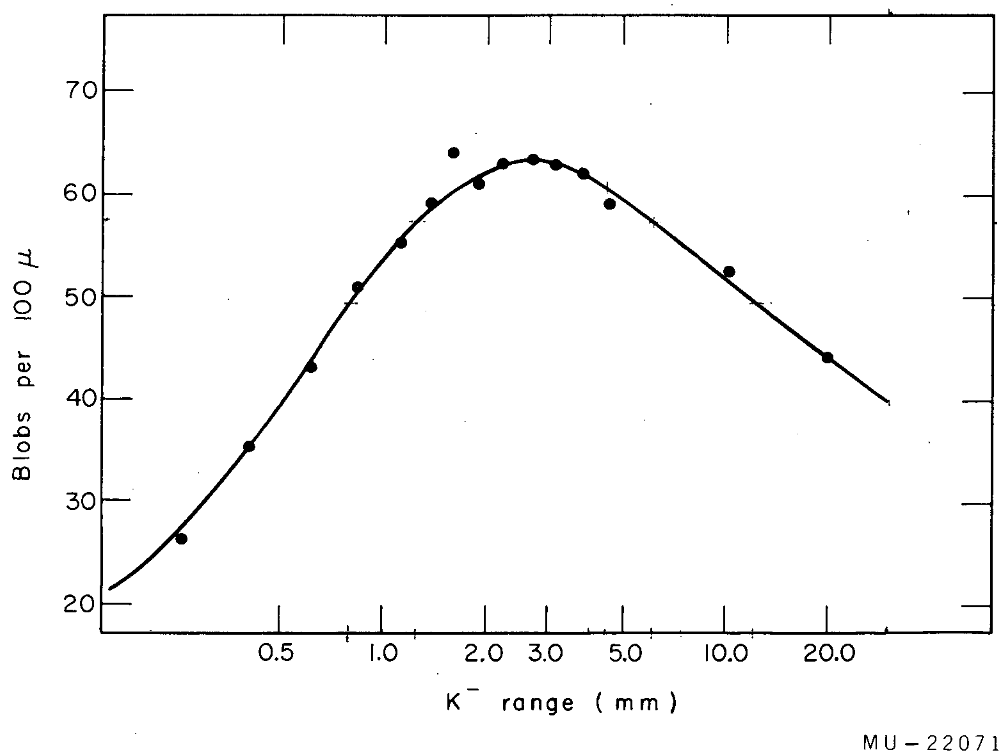


Fig. 20. $K^-$ meson residual range vs blob density. Each circle is the average value from five "flat" tracks. This curve was used to establish $B_{max}$ and the value of $a$. See text.

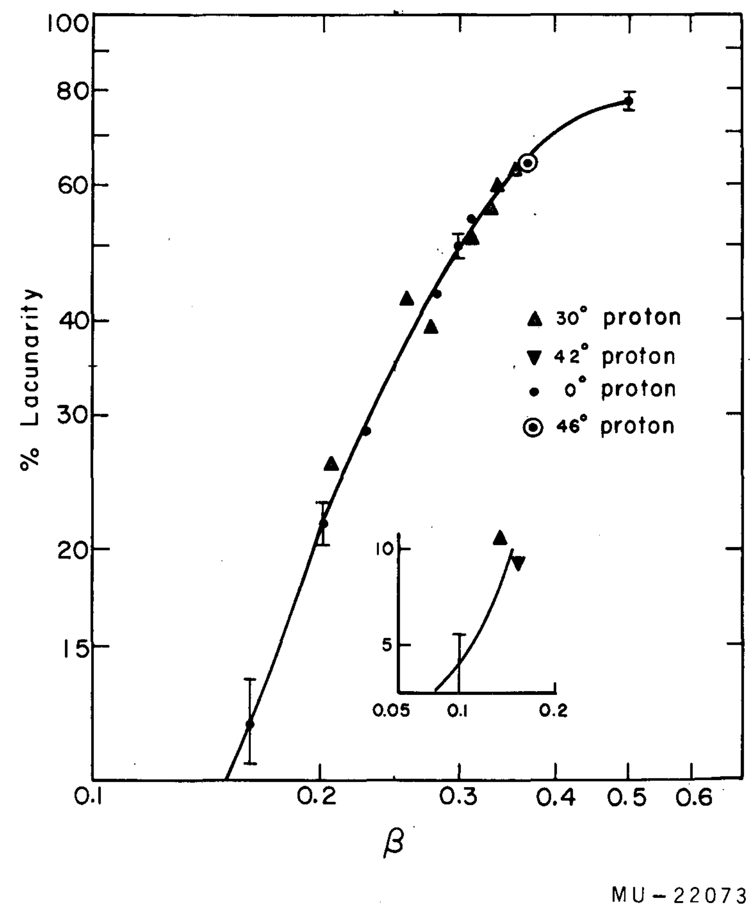


Fig. 21. Experimental curve of lacunarity vs velocity. The solid curve represents the data from five flat $K^-$ tracks. The points represent tests made with dipping protons of known velocity.

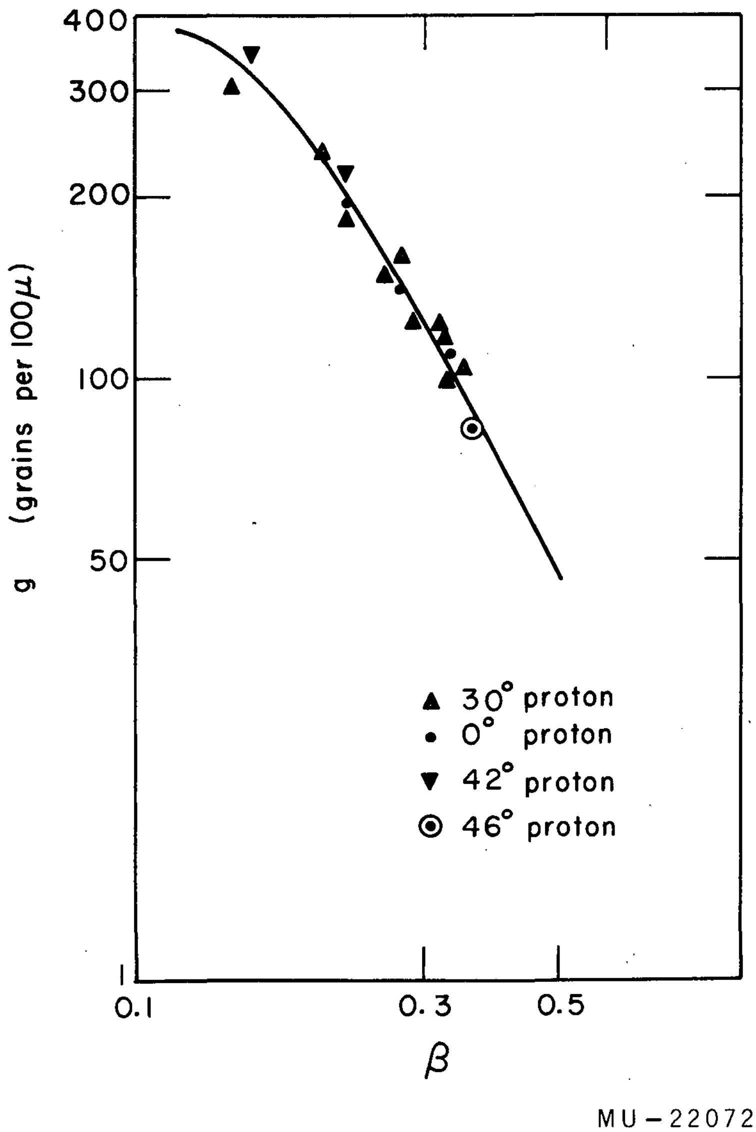


Fig. 22. Experimental curve of true grain density determined by B/L vs velocity. The solid curv- represents the data from five flat $K^-$ tracks. The points represent tests made with dipping protons of known velocity.

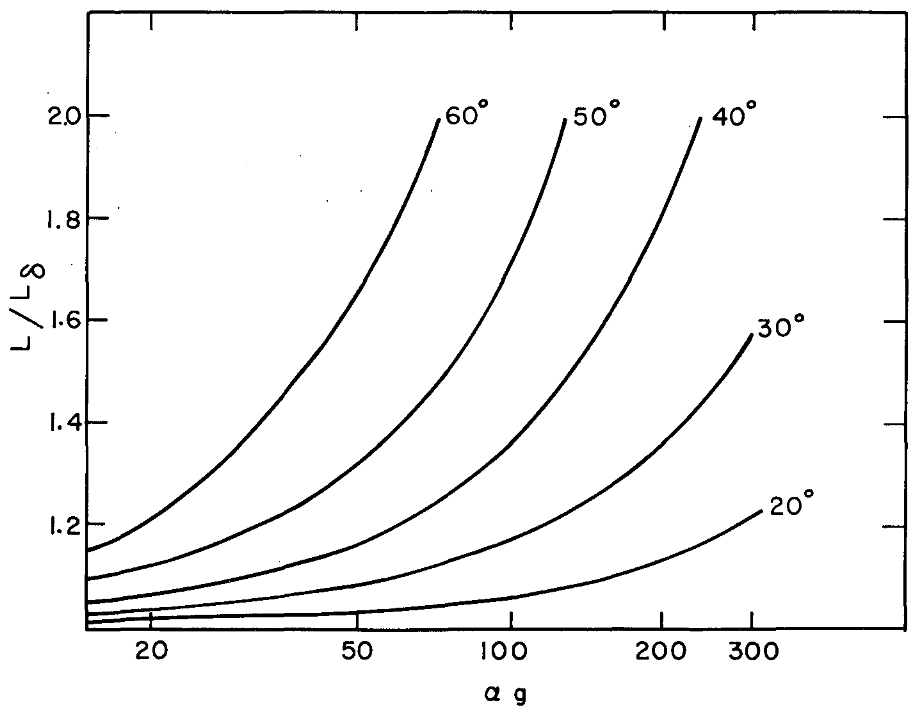


Fig. 23. The lacunarity dip correction, $L_\delta = L \exp [-ag (\sec \delta - 1)]$ . $L/L_\delta$ is plotted as a function of $ag$ for several values of the dip angle.

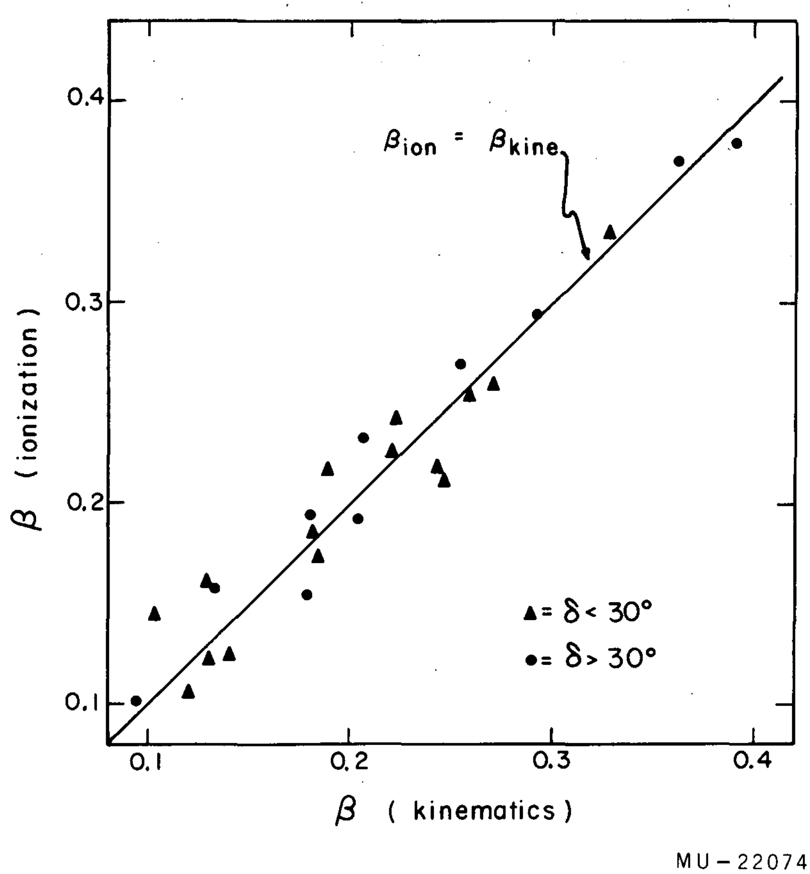


Fig. 24. Comparison of velocities determined by ionization and by decay kinematics for 25 $\Sigma^{+} \rightarrow p + \pi^{0}$ decays in flight. The average velocity for all 25 tracks differs by less than 0.5% for the two methods.

The measurements were actually performed as follows: starting at the decay point, the track was counted for 500 μ (projected) segment, or back to the $K^-$ star if the track was less than 500 μ long. If the particle passed through more than one pellicle, counting was discontinued about 10 μ from the surface and resumed about 10 μ into the next pellicle. The velocity at the midpoint of the measured segment was determined from both L and B/L and the velocity at the decay point calculated. If the curves of L and B/L did not give consistent estimates of velocity, the data were discarded and another segment of the track was measured if possible. Of 76 hyperon tracks measured, only four give inconsistent values of L and B/L, and these all had dip angles > 45 deg.

## ACKNOWLEDGMENTS

I am indebted to Dr. Walter H. Barkas for suggesting and guiding this research, and to Dr. Robert L. Thornton for his interest and encouragement.

I wish to thank all the scanners who participated in this program. Particular thanks are due Miss Ernestine Beleal, Mrs. Penny Vedder, and Mrs. Hester Yee for most of the pion range measurements, and Mr. Alan R. Betz for all the ionization measurements described in the Appendix.

To Mrs. Penny Vedder I express my gratitude for her assistance and advice concerning the IBM 650 programs.

My appreciation is due Mrs. Marilyn Mollin for a great deal of help checking the data and carrying out numerical calculations.

My appreciation is also due the members of the Barkas Physics Research Group, all of whom contributed valuable discussions and advice concerning various aspects of this research.

I wish to thank Dr. Stanley C. Freden and Dr. R. Stephen White for the use of the M stack and their data concerning the collinear events.

Finally, my deepest appreciation to my wife, Jodie, without whose help it would have been impossible for me to carry out this research.

This work was done under the auspices of the U.S. Atomic Energy Commission.

## REFERENCES


1. J. Hornbostel and E.O. Salant, Phys. Rev. 98, 218 (1955).
2. W.W. Chupp, G. Goldhaber, S. Goldhaber, and F.H. Webb, Phys. Rev. 100, 959A (1955).
3. C.E. Violet, F.C. Gilbert, and R.S. White, Phys. Rev. 100, 1803A (1955).
4. W.W. Chupp, G. Goldhaber, S. Goldhaber, and F.H. Webb, in Physics Division Quarterly Report, UCRL-3593, Nov. 1956.
5. J. Steinberger, in Proceedings of the Sixth Annual Rochester Conference on High Energy Physics (Interscience Publishers, Inc., New York, 1956).
6. W.H. Barkas, W.F. Dudziak, P.C. Giles, H.H. Heckman, F.W. Inman, C.J. Mason, N.A. Nickols, and F.M. Smith, Results from an Enriched Negative K-Meson Beam, UCRL-3627, Dec. 1956.
7. Walter H. Barkas and Arthur H. Rosenfeld, Data for Elementary Particle Physics, UCRL-8030, March 1958.
8. Walter H. Barkas and Arthur H. Rosenfeld, Data for Elementary Particle Physics, UCRL-8030 Suppl., Oct. 1960. This paper contains the data of this thesis.
9. D.A. Glaser, M.L. Good, and D.R.O. Morrison, in Proceedings of the 1958 Annual International Conference on High-Energy Physics at CERN (CERN, Scientific Information Service, Geneva 23, Switzerland), p. 270.
10. G.A. Snow, in Proceedings of the Seventh Annual Rochester Conference on High-Energy Physics (Interscience Publishers, Inc., New York, 1957), p. VIII-14.
11. R.G. Glaser, N. Seeman, and G.A. Snow, Phys. Rev. 107, 277 (1957).
12. J.H. Davies et al., Suppl. Nuovo cimento 4, 472 (1956).
13. W.F. Fry, J. Schneps, G.A. Snow, M.S. Swami, and D.C. Wold, Phys. Rev. 107, 257 (1957).

14. S.C. Freden, F.C. Gilbert, and R.S. White, Bull. Am. Phys. Soc. 3, 25 (1958).

15. W. Koch, M. Nikolic, M. Schneeberger, and H. Winzeler, Helv. Phys. Acta 32, 549 (1959).

16. M.F. Kaplon, A.C. Melissinos, and T. Yamanouchi, Ann. Phys. 9, 139 (1960).

17. D. Evans et al., ($K^-$ Collaboration, Part III), Nuovo cimento 15, 873 (1960).

18. S.C. Freden, H.N. Kornblum, and R.S. White, Nuovo cimento 4, 611 (1960).

19. Data collected by D.A. Glaser for the 1959 Kiev Conference on High Energy Physics (unpublished).

20. F.S. Crawford, Jr., M. Cresti, M.L. Good, G.R. Kalbfleisch, M.L. Stevenson, and H.K. Ticho, Phys. Rev. Letters 1, 511 (1958).

21. P. Nordin, J. Orear, L. Reed, A.H. Rosenfeld, F.T. Solmitz, N.D. Taft, and R.D. Tripp, Phys. Rev. Letters 1, 514 (1958).

22. J. Leitner, P. Nordin Jr., A.H. Rosenfeld, F.T. Solmitz, and R.D. Tripp, Phys. Rev. Letters 3, 186 (1959).

23. Peter C. Giles, Masses and Decay Processes of Charged Hyperons (Thesis), UCRL-8007, Oct. 1957.

24. Norris A. Nickols, The Lifetime and Decay Modes of Negative K Mesons (Thesis), UCRL-8692, Sept. 1959.

25. Conrad J. Mason, The $\Lambda$ - Hyperon Mass and Energy Spectrum from the Nuclear Capture of Negative K Mesons (Thesis), UCRL-9297, July 1960.

26. John N. Dyer, Analysis of the Bevatron $K^-$ Beam by Means of an Emulsion Stack, UCRL-8364, July 1958.

27. John N. Dyer, Analyses of the $K^-$ Beam Transmitted by the Murray Spectrometer, UCRL-8364 Suppl., Jan. 1959.

28. N. Horwitz, J.J. Murray, R.R. Ross, and R.D. Tripp, 450-Mev/c $K^-$ and $\bar{p}$ Beams at the Northwest Target Area of the Bevatron Separated by the Coaxial Velocity Spectrometer, UCRL-8269, June 1958.

29. Walter H. Barkas, The Range-Energy Relation in Emulsion, Part 2: The Theoretical Range, UCRL-3769, April 1957.
30. C. J. Mason and W. H. Barkas, A Microscope with Automatic Coordinate Readout Adapted for Calculating Particle Ranges, UCRL-8306 Abstract, May 1958.
31. W. H. Barkas, F. M. Smith, and W. Birnbaum, Phys. Rev. 98, 605 (1955).
32. Ladislav Rob and Zdenek Korbel, Nuclear Phys. 13, 300 (1959).
33. H. H. Heckman, B. L. Perkins, W. G. Simon, F. M. Smith, and W. H. Barkas, Phys. Rev. 117, 544 (1960).
34. W. H. Barkas, The Range-Energy Relation in Emulsion, Part 1: Range Measurements, UCRL-3768, April 1957.
35. B. Bhowmik, et al. ($K^-$ Collaboration, Part II), Nuovo cimento 14, 315 (1959).
36. M. S. Swami, Phys. Rev. 114, 333 (1959).
37. R. S. White, in Proceedings of the Seventh Annual Rochester Conference on High-Energy Physics (Interscience Publishers, Inc., New York, 1957) p. VIII-31.
38. W. F. Fry et al., Phys. Rev. 103, 226 (1956).
39. W. F. Fry et al., Phys. Rev. 104, 270 (1956).
40. M. S. Bartlett, Phil. Mag. 44, 249 (1953).
41. E. Amaldi, Suppl. Nuovo cimento 2, 253 (1955).
42. C. Franzinetti and G. Morpurgo, Suppl. Nuovo cimento 6, 577 (1957).
43. R. G. Glasser, N. Seeman, and G. A. Snow, NRL Quarterly on Nuclear Science, April 1960.
44. G. Quarini, A. Quarini Vignudelli, G. Dascolo, and S. Mora, Nuovo cimento 14, 1179 (1959).
45. R. F. Behrends, Phys. Rev. 111, 1691 (1958); P. Prakash and A. H. Zimerman, Nuovo cimento 11, 869 (1959).
46. A. H. Rosenfeld (Lawrence Radiation Laboratory), private communication.
47. Walter H. Barkas, Emulsion Statistics, UCRL-8687, March 1959. Walter H. Barkas, Emulsion Track Structure, UCRL-9181, June 1960.